N° ordre ……..…../FHC/UMBB/2012

REPUBLIQUE ALGERIENNE DEMOCRATIQUE ET POPULAIRE

MINISTERE DE L'ENSEIGNEMENT SUPERIEUR ET DE LA RECHERCHE SCIENTIFIQUE

UNIVERSITE M'HAMED BOUGARA BOUMERDES

FACULTE DES HYDROCARBURES ET DE LA CHIMIE

Mémoire de Magister

Présenté par :

MELLATI Meftah

En vue de l'obtention du diplôme de **MAGISTER** en :

Filière : Génie Electrique et Electrotechnique

Option : Infotronique

Negative Bias Temperature Instability Modeling for Pure-SiO_2

Devant le jury composé de :

Dr. KHELLAF Abdellah	Directeur de recherche	CDER	Président
Dr. NADJI Becharia	Maître de conférences A	UMBB	Examinateur
Dr. HABI Idir	Maître de conférences A	UMBB	Examinateur
Dr. BENTARZI Abdelhamid	Maître de conférences A	UMBB	Examinateur
Dr. KRIBES Youcef	Maître de conférences A	UMBB	Rapporteur

Année Universitaire 2011/2012

ABSTRACT

Negative Bias Temperature Instability (NBTI) is a serious degradation mechanism in nanoscale devices and circuits. It impacts mainly P-channel devices by generating traps at the Si/SiO_2 interface as well as in the oxide bulk. These generated traps cause the degradation of the most important transistor parameters such as threshold voltage, saturation current and channel mobility. Since the improvement of devices and circuit performance is the main target in Nanotechnology, investigating the physics of the NBTI and its modeling is essential and highly useful. In this thesis, the study of NBTI degradation for pure-SiO_2 is undertaken and it is demonstrated that for pure-SiO_2 only one mechanism is behind the degradation. This mechanism is related to $P_b$centers creation and hydrogen species diffusion into the oxide. The Reaction-diffusion framework which is widely used for modeling NBTI is investigated. Nevertheless the validity of R-D model is put under question by many researchers due to its failure in predicting some important NBTI behavior. The proposed model is an amelioration of the classical R-D by modifying some assumptions used in the classical R-D. The proposed model takes into consideration the non-instantaneous transformation of H to H_2as well as the diffusion of the latter into the polysilicon gate. COMSOL Multiphysics is used to simulate the model and the obtained results demonstrate the validity of the model.

Key word: MOSFET reliability, Negative Bias Temperature Instability (NBTI), oxide defects, Reaction-diffusion model.

Résumé

La dégradation du transistor à effet de champ (MOSFET), soumis aux contraintes de température et de polarisation négative, communément appelée Negative Bias Temperautre Instability (NBTI) est un problème sérieuxde fiabilité dans les circuits et les composants microélectroniques. Le NBTI dégrade surtout le transistor à canal P par la génération des pièges de trous à l'interface entre Si et SiO_2 ainsi qu'à l'intérieur de l'oxyde. Ces pièges provoquent la dégradation des paramètres du transistor les plus importants tel que la tension de seuil, le courant de saturation et la mobilité des porteurs dans le canal. Parce que le but ultime de la nanotechnologie est d'améliorer la performance des composants et des circuits intégrés, la compréhension de la physique du NBTI et sa modélisation et très essentielle. Dans cette thèse, ladégradation NBTI est étudiée en détail pour les transistorsà SiO_2pure. Il estdémontré qu'un seul mécanisme est à l'origine de la dégradation NBTI. Ce mécanisme est dû à la création descentres $P_b$et à la diffusion d'hydrogène dans l'oxyde. Le modèle de Réaction-Diffusion qui est largement utilisée pour décrire le NBTI est examiné en détail. Néanmoins la validité du R-D modèle est remise en cause par certains chercheurs à cause de non prédiction de quelques importantes caractéristiques du NBTI. Le modèle proposé améliore celui du R-D en prenant en considération ses lacunes et modifiant certaines hypothèses utilisées dans le R-D classique. Dans le modèle proposé, la transformation non instantanée de H à H_2 ainsi que la diffusion de ce dernier dans la gâchette à poly-silicium sont prises en compte. Enfin, pour vérifierla validité du model proposé, il est simulé dans COMSOL Multiphysics et comparé avec le R-D classique.

Mots clés: Fiabilité des transistors MOSFET, Contraintes de température et de polarisation négative (NBTI), Défaut d'oxyde, Reaction-diffusion model.

المُلخَّصُ

إنَّ تَدَهْورَ المِقْحَل (الترنزيستور) MOSFET عِنْدَ تَعَرُضِهِ لِإرْهَاقٍ مِنْ حَرَارَةٍ وَ اسْتِقْطَابٍ سَالِبٍ, ظَاهِرَةٌ يُطْلَقْ عَلَيْهَا الإخْتِلَالُمِنْ الحَرَارَةِ وَالِاسْتِقْطَابِ السَالِبِ (NegativeBiasTemperatureInstability), هَذَا التَدَهْورُ يُعْتَبَرُ مِنَ المَشَاكِلِ العَويصَةِ التِي تُهَدِدُ كَفَاءَةَ الدَارَاتِ المُدْمَجَةِ وَ مُكَونَاتِهَا النَانُو مِتْريَّةٌ. NBTI يُؤَثِرُ خُصُوصًا عَلَىالتَرَنْزيسْتُور ذِي القَنَاةِ مِنْ نَوع Pوَهَذَا عَنْ طَرِيق تَكْوِين عُيُوبٍ عِنْدَ سَطْح الإلتِقَاء بَيْنَ السِلِيسْيُوم (Si) وَثَانِي أُوكْسِيدِ السِلِيسْيُوم (SiO_2) أوْ دَاخِلَ نَسِيجِ الأُكْسِيدِ نَفْسِهِ. هَذِهِ العُيُوبُ تُؤَثِرُ عَلَى أهَمِّ خَصَائِص الترَنْزيسْتُور مِنْهَا كُمُونُ ضَغْطِ العَتَبَةِ, تَيَارُالإشْبَاع وَ مَدَى حَرَكِيَّةُ القَنَاةِ. عِلمًا أنَّ الهَدَفَ الذِي تَصْبُوا إلَيْهِ صِنَاعَةُ النَانُو تَقْنِيَّةٌ هُوَتَحْسِينُ كَفَاءَةِ الدَارَاتِ المُدْمَجَةِ وَ مُكَونَاتِها, لِكَيْ يَتِمَّ هَذَا يَجِبُ عَلَيْنَا أوَلًا فَهْمَ ظَاهِرَةNBTI وَ نَمْذَجَتُهَا. لِهَذَا الهَدَفِ يَأْتِي هَذَا البَحْثُ الذِي نُخَصِصُهُ لِدِرَاسَةِ هَذِهِ الظَاهِرَةِ فِي الأُكْسِيدِ الخَالِص مِنَ الشَوَائِبِ. لَقَدْ بَرْهَنْتُ عَلَي وُجُودِ آلِيَّةٍ وَاحِدَةٍ تَقِفُ خَلْفَNBTI مُرْتَبِطَةٌ بِنُشُوءِالمَرَاكِزِ مِنْ نَوْعِP_b وَ انْتِشَار الهَيْدُرُوجِينَ فِي الأُكْسِيدِ. تُعْتَبَرُ أرْضِيَّةُ التَفَاعُل-الانْتِشَار الحُلُولِي مِنْ أكْثَر الأرْضِيَّاتِ اسْتِعْمَالًا لنَمْذَجَةNBTI لَكِنَّهَا تَتَعَرَضُ لِكَثِيرٍ مِنْ الانْتِقَادَاتِ لِعَدَمِ تَمَكُنِهَا مِنْ مُحَاكَاتِ بَعْضٍ مِنْ الخَصَائِص الهَامَةِ لNBTI. النَمُوذَجُ المُقْتَرَحُ فِي هَذِهِ المُذْكِرَةُ يُحَسِنُ نَمُوذَجَالتَفَاعُل-الإنْتِشَار الكَلاسِيكِيَّ وَهَذَا بِالأَخْذِ بِعَيْنِالاعْتِبَار بَعْضَ الفَرَضِيَاتِ التَسْهِيلِيَّةِ المَوْجُودَةِ فِي نَمُوَذجِالتَفَاعُل-الإنْتِشَار الكَلاسِيكِيِّ. فِي النَمُوذَج المُقْتَرَح نَأْخُذُباعْتِبَارِنَا التَحَوُلَ الغَيْرَ لُحْظِيّ مِنْ ذَرَةِ الهَيْدُرُوجِين إلَى جُزَيءِ الهَيْدُرُوجِين وَالانْتِشَارَ الحُلُولِيَّ لِهَذَا الأخِير فِي البَوابَةِ المُتَعَدِدَةِ السِلِيسْيُوم. فِي الأخِيرِيَتِمُ إخْتِبَارُ النَمُوذَج المُقْتَرَح عَنْ طَرِيقِمُحَاكَاتِهِ فِي بَرْنَامَج COMSOL Multiphysics, نَتَائِجُالمُحَاكَاتِ تُبَيِّنُ قِيمَةَ النَمُوذَج المُقْتَرَح.

الكلمات المفتاحية: تَدَهْورَ المِقْحَل (الترنزيستور) MOSFET , الاسْتِقْطَابِ سَالِبٍ, ظَاهِرَةٌ يُطْلَقْ عَلَيْهَا الإخْتِلَالُ مِنْ الحَرَارَةِ وَ الِاسْتِقْطَابِ السَالِبِ, عُيُوبِالأُكْسِيدِ, نَمُوذَجَ التَفَاعُل-الإنْتِشَار.

ACKNOWLEDGMENTS

First, I would like to express my deep gratitude to my thesis mentor **Dr. Y. KRIBES** for the continued follow-up, collaboration and support he has had during the course of this work. I want to thank him especially for his willingness to comment and discuss results and ideas, and the fruitful discussions that have shaped this work.

Also, I wish to warmly thank **Dr. B. NAJI** responsible the INFOTRONQUE option who gave me the chance to get into this wonderful world of scientific research.

I cannot forget to thank my family, my friends for their encouragement and unconditional support to perform this work.

Finally, I have to thank my colleagues in the group of INFOTRONIC, I appreciate their friendship.

CONTENTS

LIST OF FIGURES

CHAPTER I

INTRODUCTION

Microelectronics has greatly contributed to the technological revolution of the late twentieth century. It has become highly incorporated into our society, permeating many parts of our lives. Computers, Internet, medical devices, air traffic control, financial exchanges, microscopes and cell phones are all the progress that has radically changed the way the human beings live.

All these technological advances have been financially and physically possible only through miniaturization of the basic components of the integrated circuits (IC). Actually, it is the device scaling that has been the engine driving the integrated circuit microelectronics revolution as described by Moore's Law. The critical elements in device scaling are the gate dielectric thickness and the channel length. These dimensions have changed from their early 1970's values of 50-100 nm and 75 nm respectively, to 1.1-1.6 nm and 45 nm nowadays. The miniaturization allowed, for example, the drastic volume reduction of the first computers that were very huge in spite of very basic functions they intended to perform.

Other advantages of miniaturization are the reduction of cost and power consumption (smaller is faster, cheaper and lower in power). This reduction in cost per transistor has allowed the integration of a large number of transistors per chip therefore allowing the manufacturing of complex electronic circuits.

Initially, dielectric thickness and operating voltage were to be scaled at the same rate so that the electric field across the gate dielectric remained constant; nevertheless, the industry soon adopted a constant voltage mode of scaling. The higher electric field associated with constant voltage scaling degraded the oxide integrity, and new process improvements were soon required.

The history of the semiconductor industry has revealed that the miniaturization tendency has been constrained by the ability of the fabricated transistors to withstand the increasing operating stresses. The gate dielectric may indeed be the key structural element in the reliability of MOSFET transistor. It is the smallest dimensional element in a transistor and yet has to withstand the highest electric field. It must have low levels of fixed charge (~ 5 x 10^{10} cm^{-2}) and interface states (~ 5 x 10^{10} cm^{-2} eV^{-1}) and must remain reliable after years of high field stressing (~ 10 years) since it occupies a large fraction of the total chip area and thus can dominate yield. The silicon dioxide (SiO_2) possesses those attributes to the extent that no other material does. The qualities of SiO_2 have made from it the mainstay of the industry for the past 40 years.

As the miniaturization has stepped into deep nanometer arena major reliability issues arose. Some of them are Hot Electron degradation, Electromigration, Oxide Breakdown (TDDB), Bias Temperature Instability (BTI), Latchup and Soft errors. These problems have limited the miniaturization and pushed researchers to look up for new alternative material.

In the 1960s, one micrometer at that time was considered as the limit due to short-channel effects and optical problems in the manufacturing steps using lithography. During 1970s, the short channel effect was overpassed and 500 nm was considered to be the physical limit because of the increased resistance source / drain. The switch from buried channel to surface channel further boosted the miniaturization. At the end of 1970, the limit was 250 nm for reasons of leakage (tunneling current) through the gate oxide and dopant fluctuation in the channel. Once the problem of leakage current has been overcome, in the 1980s, 100 nm was considered the physical limit as many difficulties prevented the reduction of physical parameters of the MOSFET (Metal-Oxide-Semiconductor Field Effect

Transistor). Finally, 10 nm has long been accepted as the physical limit for many reasons including that of the tunneling current between the source and the drain.

One of the most longstanding reliability problems that now is limiting the downscaling of the oxide is Negative Bias Temperature Instability (NBTI). It is a major reliability concern for modern complementary metal oxide silicon technology. It manifests itself as a shift in threshold voltage (V_T) and a degradation in saturation drain–current ($I_{D,sat}$) in p-channel metal oxide silicon field effect transistors (pMOSFETs) subjected to negative gate bias at moderately elevated temperatures. It was observed as early as 1967 by Deal et al., but an apparently consistent explanation was only made much later in 1977 by Jeppson and Svensson, based the Reaction-Diffusion model.

In this work NBTI is subjected to a close investigation. In the purpose to end out with a new model, the thesis is structured such as to present the issue form the fundamental basic of the oxide growth technique and the most important electrical defects through presenting the state-of-the-art definitions and understandings of NBTI physical degradation and model, ending with new proposed model and its simulation.

Chapter two presents the fundamental techniques used in the SiO_2 growth over Si substrate along with the nitrogen incorporation into the oxide techniques. The different oxide electrical defects at the Si/SiO_2 interface as well as in the oxide bulk are explained. Based on these defects the macroscopic picture of proposed model is given.

Chapter three focuses on the NBTI distinguishing it from other degradation mechanisms. Some techniques used in NBTI measurements are quoted highlighting their evolution from conventional Stress-Measurement-Stress (SMS) technique, known to underestimate the degradation because of its inevitable recovery, to ON-THE-FLY (OTF) method. This chapter is ended out by studying NBTI features and signatures.

Chapter four gives an overview of common NBTI models. Two well-known models are explored; the first is a hydrogen-diffusion related model known as Reaction-Diffusion model. Then second is a hole-trapping and detrapping based model known as Two-Stage model.

My contribution to the NBTI modeling is found in chapter five and six. The proposed model is based on the Reaction-Diffusion model framework. The fact that the transformation of the released H to H_2 is not instantaneous, together with the fact that H_2 diffusion mainly occurs in the polysilicon are taken in consideration. The proposed model is simulated using COMSOL Multiphysics.

CHAPTER II

DEFECTS IN THE Si-SiO_2 SYSTEM

II.1 INTRODUCTION

Silicon dioxide (SiO_2) is one of the most important elements in the manufacture of semiconductors as it has played a crucial role in the development of planar semiconductor processing. In fact, the widespread use of silicon in the microelectronics industry is primarily ascribed to its silicon dioxide. SiO_2 is easily grown over Si and the obtained layer as well as the interface between Si and SiO_2 are of enough quality to allow the fabrication of reliable MOS-based devices.

Most of the reliability problems in MOS -based devices are related to defects in the oxide. The presence of defects is detrimental to both production efficiency and long term reliability. Therefore, the study of the microscopic structure of these defect and their properties is essential to understand the nature of any reliability issue.

For this purpose, Chapter II is devoted to, briefly, overview Si oxidation process, highlighting the rapid thermal growth and nitrogen introduction. In the same context insights are made on the microstructure of Si-SiO_2 interface and bulk SiO_2 defects.

II.2 OXIDATION PROCESS

Although several methods such as dry and wet thermal oxidations, plasma anodization, vapor phase reaction, and the wet anodization have been developed and implemented for the growth of silicon dioxide films, the dominant technology is the thermal oxidation because the gate oxide obtained is of a good quality and thermal oxidation is the simplest among its competitors [1][2][3].

Thermal oxidation of SiO_2 is obtained by exposing the silicon substrate to an oxidizing environment of O_2 or H_2O at high temperatures, producing oxide films with thicknesses ranging from 60 to 10,000 Å. The oxidation of silicon is not difficult because silicon has a high affinity to form a stable oxide even at room temperature [1]. The high temperature used in thermal oxidation serves primarily as an accelerator of the oxidation process, resulting in thicker oxide layers per unit time.

Depending on which oxidant species used (O_2 or H_2O), the thermal oxidation of SiO_2 may either be in the form of dry oxidation (wherein the oxidant is O_2) or wet oxidation (wherein the oxidant is H_2O). The reactions for dry and wet oxidations are governed by the following equations:

- For dry oxidation:

$$\mathrm{Si\ (solid)} + \mathrm{O_2\ (vapor)} \rightarrow \mathrm{SiO_2\ (solid)}$$

- For wet oxidation:

$$\mathrm{Si\ (solid)} + \mathrm{2H_2O\ (vapor)} \rightarrow \mathrm{SiO_2\ (solid)} + \mathrm{2H_2\ (vapor)}$$

II.2.1 Rapid Thermal Oxidation

Conventional thermal oxidation has undesirable effects on the device quality such as the high impurity distribution in the bulk of silicon and at the Si/SiO_2, because of the use of high temperature for long periods. It is important to control and minimize these effects. This task is achieved by precisely controlling the oxidation temperature using the rapid thermal oxidation (RTO) technique.

During RTO, the wafer is rapidly heated from a low to a high processing temperature (T > 900°C). The wafer remains at this elevated temperature for a short time and is, then, brought back rapidly to a low temperature. Typical temperature rates range from 10 to 350°C/s, compared with about 0.1°C/s for conventional thermal oxidation. RTO reduces the ramp-up and ramp-down durations. The RTO durations at high processing temperatures vary from 1s to 5 min. This makes RTO very suitable to grow thin oxide films (< 40 nm), where a precise temperature control and short oxidation times are important to control the impurity distribution.

II.2.2 Oxide Nitridation

SiO_2 has been the main material for gate dielectrics for more than three decades. Increasing problems related to scaling effects such as polysilicon dopant penetration and direct tunneling of free carriers through the ultrathin oxide films dictated the search for new materials for future gate dielectrics with better diffusion barrier properties and higher dielectric constants (High-K dielectrics). Ultrathin silicon oxynitrides (SiO_xN_y) are revealed to be good candidates to replace pure SiO_2.

Nitrogen may be incorporated into SiO_2 using either thermal oxidation/annealing or plasma nitridation methods.

a) Thermal Nitridation Oxidation

In thermal nitridation oxidation (TNO) the nitrogen species such as nitric (NO), nitrous (NO_2) or Ammonia (NH_3) are added to the oxidation ambient during the SiO_2 growth or introduced to the post-oxidation anneal. NO is the main species responsible for nitrogen incorporation into the film. A build-up of interfacial nitrogen and bulk nitrogen throughout the film is enhanced during the silicon oxynitridation. The nitrogen concentration and its distribution through the oxide are very sensitive to processing parameters. The interfacial nitrogen concentration in N_2O nitrided oxides is typically less than that of NH_3 and NO nitrided oxides.

b) Plasma Nitrided Oxidation

Plasma nitrided oxidation (PNO) process has been established as a standard method of forming ultrathin gate. The advantage of the PNO of SiO_2 is in its ability to control the dielectric layer thickness as well as the content and location and/or profile of nitrogen incorporation independently and precisely. In addition, since it is plasma, a non-thermal process, two benefits are gained compared with the thermal processes:

- The nitrogen can be incorporated much more precisely than for the thermal processes,
- The profile of the nitrogen can be carefully engineered.

II.3 ANNEALING AMBIENT

The annealing step is very crucial for the quality of the oxide. Its greatest impact is the reduction of charge trapping and interface trap density whether the oxide is a thermal oxide or a plasma deposited oxide. When the oxide annealing is performed immediately after the oxidation process, it is called post-oxidation anneal (POA) and when it is performed after the metal or polysilicon gate has been formed it is referred to by post-metal anneal (PMA). The POA ambient is typically N_2 or Ar. The PMA ambient is typically forming gas (mixture of N_2 and H_2).

II.4 STRUCTURE OF SiO_2

The silicon dioxide obtained after the oxidation process is amorphous SiO_2. It can be described as a network short-range order of tetrahedral cells, with four oxygen atoms surrounding a silicon atom, as shown in Figure II.1.a. The silicon atoms are at the center of each tetrahedron. The length of a Si-O bond is 0.162 nm and the normal distance between the oxygen ions is 0.262 nm. The network structure of SiO_2 is shown in Fig.II.1.b. In an ideal network, vertices of the tetrahedra are linked by a common oxygen atom called Oxygen Bridge (OB) [4].

An effective band-gap exists in amorphous SiO_2 which depends on the degree of perfection of the oxide network. The value of band-gap decreases as the disorder increases. The

experimental E_G values of SiO_2 usually range from 8.1 eV to 9 eV, depending on the processing conditions [4].

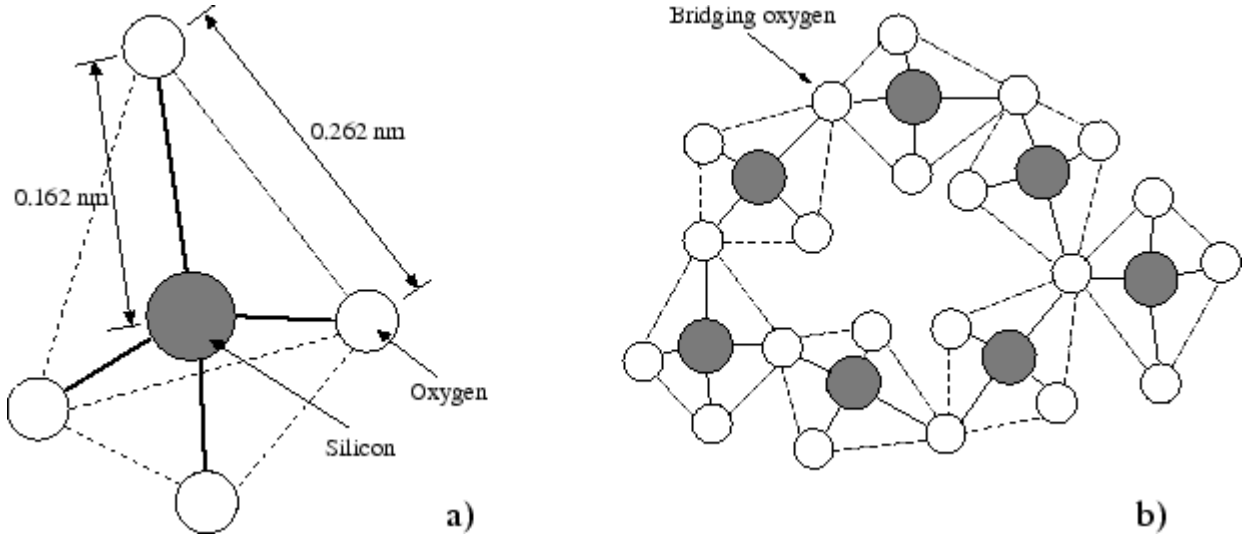

Figure II.1: a- Structure of SiO_2 unit cell and **b**-structure of SiO_2 network.

II.5 OXIDE AND INTERFACE DEFECTS

Pure silicon dioxide consists of a network of SiO_4 tetrahedra. These SiO_4 tetrahedra are linked to one another by shared corners, where each oxygen (O) atom forms a bridge between two Si atoms. Such shared atoms are called bridging oxygen atoms. The deviations from this regular SiO_2 distribution are referred to as defects. They include Si or O vacancies and interstitials, disordered areas with strained or dangling atomic bonds, over- and under-coordinated Si or O atoms Si-O-H bonds and weak Si-O.

II.5.1 Bulk Defects

Bulk defects are defects in the oxide located far inside the oxide. They can be charged or can be neutral and are capable of trapping electrons or holes. These bulk traps may trap free charge induced in the oxide by an ionizing radiation or a high current flow, thus affecting device performance and lifetime.

II.5.2 Interface Defects

The silicon atom possesses four valence electrons and therefore requires four bonds to fully saturate the valence shell. In the crystalline structure each silicon atom establishes bonds to its four neighboring atoms, leaving no unsaturated bonds behind. After oxidation a strained layer, induced by the lattice mismatch between the crystalline Si substrate and the SiO_2 layer, is observed and is largely controlled by the processing condition. Not all the Si bonds are passivated by an oxygen atom; there remain some dangling bonds in the order of 10^{12} $cm^{-2}eV^{-1}$. Each electrically active interface state leads to the degradation of important MOSFET parameters such as the threshold voltage, the on-current, or the surface carrier mobility. To improve the quality of interface, the number of dangling valence bonds is further reduced by annealing the interface in forming gas with hydrogen atoms. The dangling silicon bonds are passivated by forming Si-H bonds. With this treatment the amount of electrically active interface states can be reduced to around 10^{10} $cm^{-2}eV^{-1}$.

Interface traps (also called fast or surface states), unlike the other traps, are in direct electrical communication with the underlying silicon substrate. These defects create energy levels within the silicon bandgap and can be occupied depending on the silicon surface potential.

II.5.3 Border Traps

Border traps are bulk traps physically located at the vicinity of the interface. Like the interface traps, border traps can exchange charges with the underlying Si substrate [12].

II.6 ELECTRICAL PROPERTIES OF DEFECTS IN Si/SiO_2 SYSTEM

The defects in the SiO_2 as well as at the SiO_2/Si interface that are relevant for device reliability are those which are or can become electrically active. They can trap or exchange charge with the underlying Si substrate. Active defects can be neutral or charged. Neutral defects can trap charge during the device life leading to an accelerating aging and charged defects in the bulk oxide or at the interface influence the MOSFET device electrical performance. Oxygen vacancies, E' and P_b centers are the most important SiO_2 defects related to the reliability of MOS-based devices [6].

II.6.1 Oxygen Vacancy

The oxygen vacancy (Vo) is a structure of a fundamental importance for reliability issues. Vo is the lack of oxygen atom that should bridge two Si atoms. The remaining dangling bonds originating from the neighboring atoms form a common bond. This bond is associated with a trap level far below the crystalline silicon conduction band edge. In amorphous SiO_2 where the strain between the two Si atoms is not the same for all Vo defects, a continuum of energy levels is introduced in the oxide bandgap [5].

II.6.2 E' Center

The E' center, usually observed in irradiated MOS devices, consists of two Si atoms joined by a weak, strained Si–Si bond with a missing oxygen atom, sometimes referred to as an oxide vacancy. E' centers also preexist in oxide films due to the amorphous nature of SiO_2 [7].

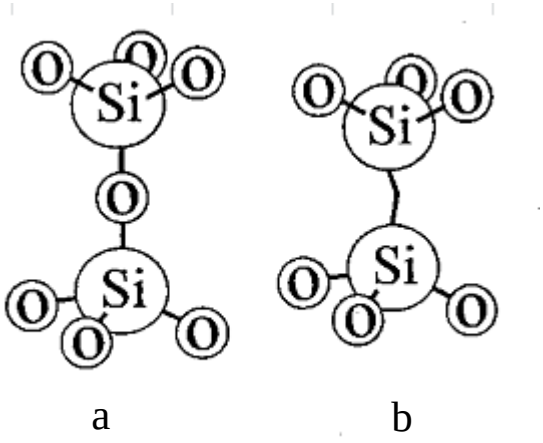

Figure II.2: a- The SiO_2 structure and **b**-The oxygen vacancy

II.6.3 E'_{δ} Center

The removal of one electron from the Vo by exciting a bonding electron to the SiO_2 conduction band or by a hole trapping causes a repulsion between both atoms, accompanied by a strong increase of the bond length. However, the common bond still persists, giving rise to defect levels, called E'_{δ}, with a wide energy distribution close to the

silicon valence band upper edge as shown in Figure II.3 [6]. Depending on their energy position with respect to the substrate Si valence band (Figure II.3), these defects behave differently. For defects energy levels which are below the upper limit of the valence band of silicon, substrate electrons can tunnel to the defect. Consequently, the energy levels will move downwards well below the valence band. The captured electron is unlikely to tunnel back to the substrate. In short, these defects remain neutral once they are discharged. Defects that are located above the silicon valence band edge, once charged by capturing a hole from the underlying Si substrate, can hardly be neutralized. Therefore, these positive charges behave like fixed positive charges [6][7].

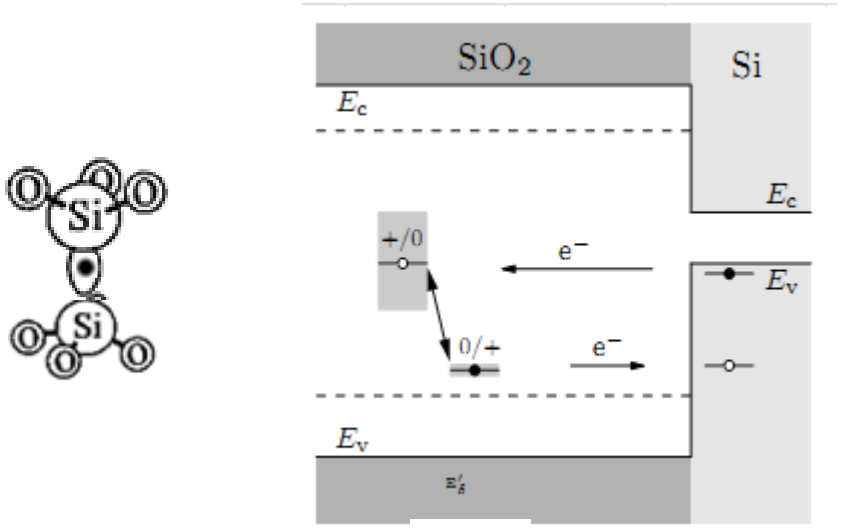

Figure II.3: a- the E'$_\delta$ configuration **b**- Schematic of defect levels arising from E'$_\delta$ (+/0 represents charged E'$_\delta$, 0/+ neutral E'$_\delta$ double sense arrow represents the energy shift after the defects are charged or neutral)

II.6.4 E'_γ Center

The E'γ center is the stable partner of the E'$_\delta$ center. One Si atom remains neutral with one electron in its external orbital oriented along the short bond direction into the vacancy. The other Si adjacent to the vacancy becomes positive charged and it relaxes away into the plane of its three neighbor oxygen. In contrast to the O vacancy, the E'γ center exhibits

only a small spread in its energy levels because the dangling bond undergoes only little relaxation. The energy levels (figureII.4) of the charged and the neutral counterpart of E'γ lie close to the conduction and valence band edge respectively. As a result, only a small thermal excitation of the majority charge carriers in the substrate is required for a tunneling process between the substrate and the defect. In this case, the band bending governs the concentrations of electrons in the silicon conduction band or holes in the silicon valence band, respectively, and as a consequence controls the corresponding tunneling rates [6][7].

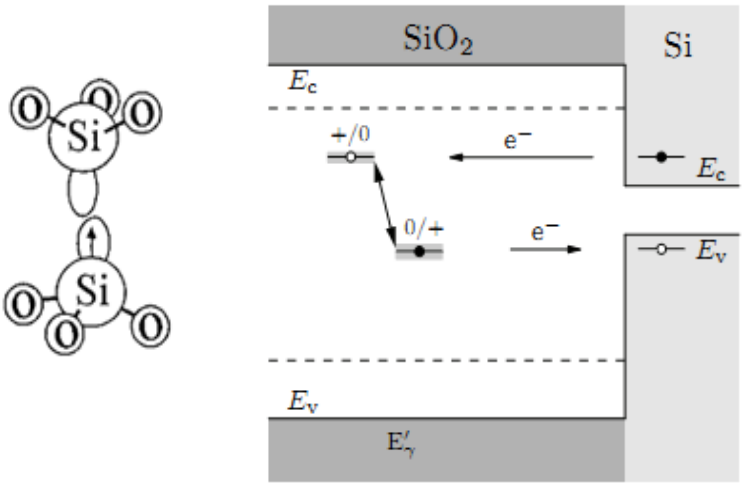

a b

Figure II.4: a- the E'γ configuration **b**- Schematic of defect levels arising from E'γ (+/0 represents charged E'γ, 0/+ neutral E'γ double sense arrow represents the energy shift after the defects are charged or neutral)

As a conclusion, the E'γ defect is a good candidate for NBTI based on hole-trapping which are capable of repeatedly exchanging electrons with the substrate.

II.6.5 P_b Center

The P_b center is a trivalent Si defect at the SiO_2/Si interface (a silicon atom bonded to three other Si atoms) with an unpaired electron in an orbital pointing out to a vacancy. It is represented by the chemical formula •Si≡Si3 [11].

P_b centers are readily generated in thermal oxides, but emerge in slightly different configurations depending on the crystallographic orientation of the Si substrate (Figure II.5). On Si(111), the P_b center is a Si atom bonded to three other Si atoms at the interface with an unpaired electron in an orbital pointing out to a vacancy, and is designated as •Si≡Si3. For the technologically important Si(100), there are two types of P_b centers. One is the Pb_0 center which is essentially similar to the P_b variant on Si(111), but with two possible orientations. The other, called the Pb_1 center, is tentatively assigned to the •Si≡Si_2O structure (i.e., a partially oxidized P_b center). These interface defects introduce energy levels in the bandgap of SiO_2 and participate in the trapping and detrapping of carriers.

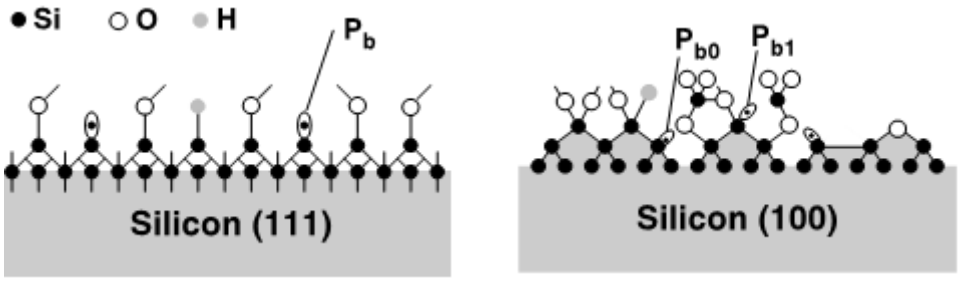

a b

Figure II.5 The Pb configuration **a-** for (111) surface **b-** for (100) surface

The P_b defect is believed to be amphoteric, that is its charge condition can be positive, negative or neutral. The P_b centers whose energy level is in the lower part of the Si bandgap are donor interface defects. They are positively charged when empty and electrically neutral when occupied by an electron. The P_b center whose energy level is in the upper part of the Si bandgap is acceptor like and is negatively charged when occupied by electron and electrically neutral when empty [7].

II.6.6 Trapping and Detrapping Process

The trapping and detrapping processes of a hole are illustrated in Figure II.6. The oxygen vacancy (A in Figure II.6) can trap a hole and transfers to an E'γ center (figureII.6.B) with a positive charge and an energy level located just above the conduction band. When positive gate bias is applied, electrons, in the Si underlying substrate, pile up and can

tunnel to the positive charged Si atom of the E'γ. The captured electron resides on this atom only for short time since this configuration of two unpaired spins in parallel is not allowed (figure II.6.C).

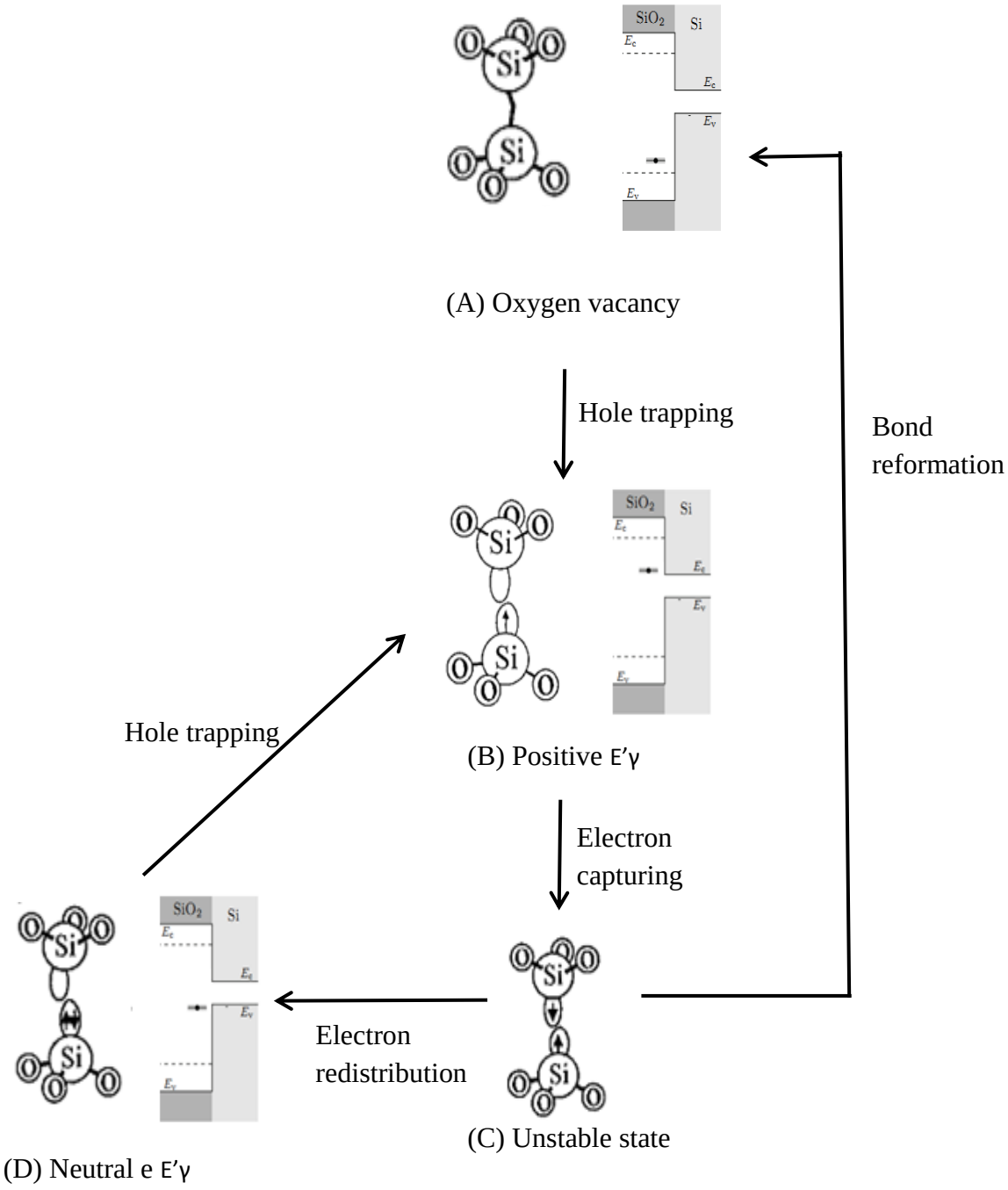

Figure II.6: Schematic description of the trapping and detrapping of a hole process.

If the E'γ defect is located far into the bulk of the oxide, the Si-Si bond would form back to its original state (Vo). On the contrary, if the E'γ defect is located near the interface, the Si-Si bond would not restructure and a neutral compensated defect is generated with its energy level shifting downward just below the valence band (Figure II.6.D). When the applied gate voltage becomes negative, the neutral compensated defect emits the trapped electron and the positive charged E'γ is formed back [7].

II.7 CONCLUSION

SiO_2 is an important element for the modern IC technology. It is easily grown over Si wafer by thermal oxidation.

Nitrogen is often added to the SiO_2 layer during processing to improve its reliability in response to the scaling side effects. Nitrogen profile in the oxide depends on the type of the oxidation used (TNO or PNO).

The oxide obtained is of enough quality to allow the fabrication of reliable oxide layer. Nevertheless some defects may exist in the bulk, interface or at the border.

The E' center family is an oxygen vacancy that losses one electron. It is a potential candidate for bulk traps and border traps.

The P_b center is an interface defect which is a dangling Si bonds at the interface. And it can exchange free carriers with the underlying Si substrate.

CHAPTER III

NBTI LITERATURE REVIEW

III.1 INTRODUCTION

Since their first commercialization, MOSFETs have taken the leading place in the microelectronic industry. This is attributed to their best reliability compared to their counterparts. To continue having this place, their reliability should be improved in response to the industry ongoing strive for scaling. The scaling tendency along with the constant operation voltage adopted in the industry has increased the oxide field and the operating temperature therefore exacerbating the reliability of the device. Impurities such as nitrogen have been added to the oxide to improve its reliability against the side effects of scaling especially for the boron penetration and carrier tunneling through the oxide. These additives are proved to enhance some MOSFET degradation mechanism.

One of the most reliability critical issues is the Negative Bias Temperature Instability (NBTI). Its first symptoms were known since the beginning of the era of microelectronics by 1960.

In this chapter, a comprehensive literature review of the NBTI degradation will be presented together with methods of assessing and extracting of parameter related to NBTI. The main NBTI key features distinguishing it from other reliability issues are studied.

III.2 DEFINITION OF NBTI

It is commonly admitted that under a constant negative gate bias stress and at high temperatures positive charges build up at the Si/SiO_2 interface and in the bulk of the oxide. The created positive charge causes the performance of p-channel MOSSFETs to degrade such as "the increase in the threshold voltage, the degradation of the mobility and transconductance".

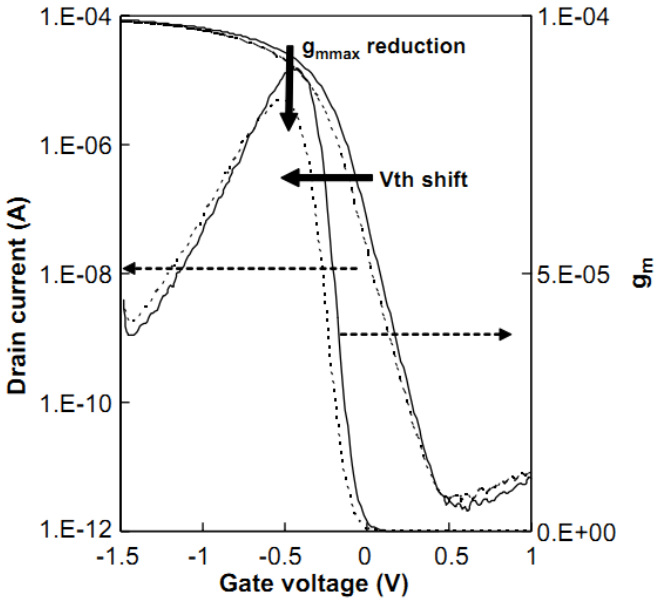

Figure III.1 I_D-V_G and g_m-V_G curves for fresh device (solid line) and after 10^4 s of NBTI stress (dashed line) for a p-MOSFET [13]

Figure III.1 shows the impact of NBTI stress on the electrical characteristics of a transistor [13]. The solid line represents the characteristics of a fresh device (before NBTI stress), and the dashed line represents those of the same device after stress. A shift of threshold

voltage and a reduction of mobility manifested by a decreasing of the transconductance are clearly shown in Figure III.1. Generally, it is observed that after an NBTI stress [14]:

- The transconductance g_m decreases,
- The linear drain current $I_{d,lin}$ and saturation current $I_{d,sat}$ decrease,
- The channel mobility μ_{eff}, degrades,
- The subthreshold slope S decreases,
- The absolute value of the threshold voltage V_T increases,

Actually the instability is observed in both configurations n-MOSFET and p-MOSFET and under positive or negative bias voltage as illustrated in Figure III.2. But p-MOSFET under negative stress is experimentally shown to be the most vulnerable device to NBTI. This is why NBTI is a reliability phenomenon which is widely related to p-MOSFET transistors.

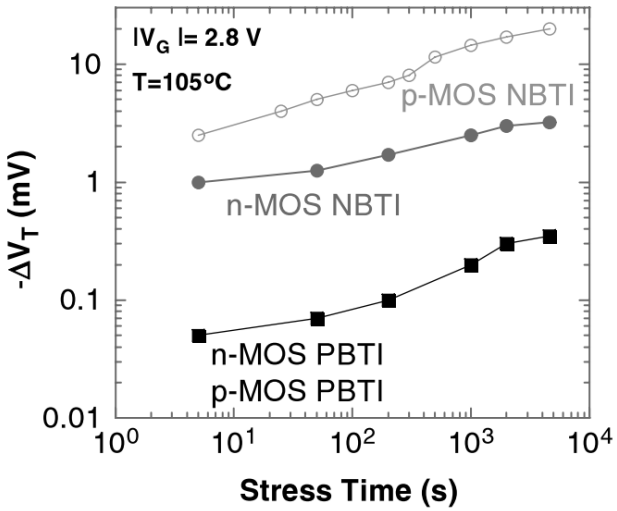

Figure III.2 Threshold voltage shift for p-MOSFET and n-MOSFET under negative and positive bias stress [11]

III.3 NBTI-RELATED PARAMETER EXTRACTION

In the experimental set-up for NBTI measurements, the substrate, the source and drain contacts are grounded while the gate is negatively biased. These bias conditions are applied

at elevated temperatures, typically ranging between 100 and 200 C°, for different periods of time. NBTI is usually monitored through the measurement of the threshold shift (ΔV_{th}) and the change of surface density of interface traps (ΔN_{it}).

III.3.1 Threshold Voltage Extraction

Many methods, for the extraction of the threshold shift, have been used such as conventional stress measurement stress method (SMS) and On-The-Fly method (OTF).

In earlier time, threshold voltage shift was extracted using the stress measurement stress method. The stress is periodically interrupted and the I_D-V_g characteristic is extracted by performing a gate voltage sweep while measuring the drain current at a slightly forward biased drain contact (linear regime). V_{th} shift is obtained by comparing the I_D-V_g characteristic before stress with the I_D-V_g characteristic obtained after stress. The fact that the stress is interrupted each time to measure V_{th} shift gives the method its name: stress measurement stress method (SMS).

The observation of post-stress recovery of NBTI [15][16] (as will be discussed later in this chapter) has complicated the threshold voltage extraction. Since then, the attention of scientists shifted towards looking for new measurement set-up where the time of measurement can be reduced or even suppressed if possible.

A method called On-The-Fly measurement was developed. The transconductance g_m, the drain current in the linear regime $I_{d,lin}$, and the threshold voltage shift ΔV_T can be extracted while keeping the gate stress voltage nearly constant.

In the On-The-Fly measurement [13], the source and bulk contacts are grounded while the drain contact is slightly biased with typically −25mV. One first measures the pre-stress V_{th} (V_{th0}) by I_D-V_G sweep and drain current (I_{D0}) at t_0 (time-zero delay which is ≥ 1ms for the Slow-OTF and ~1μs for the Fast-OTF) [17]; then the stress at the gate contact is permanently applied and superimposed upon pulses which are small compared to the stress voltage. The transconductance g_m of the transistor, which is defined as the change in drain current as a result of a change of gate voltage, can then be extracted as:

$$g_m = \frac{\partial I_{d,lin}}{\partial V_g} = -\frac{\partial I_{d,lin}}{\partial V_{th}} \quad \text{(III. 1)}$$

From this relation ΔI_D is obtained. The threshold voltage shift can then be extracted using [13]:

$$\Delta V_{th} = \left| \frac{(V_G - V_{th0})\Delta I_D}{I_{D0}} \right| \quad \text{(III. 2)}$$

It is important to know that the measured I_{D0} is assumed to be the "degradation-free" I_D, based upon which subsequent I_D shifts are calculated. Due to a finite delay before I_{D0} measurement can be made following the application of the gate stress voltage, degradation may already have occurred, resulting in an underestimated degradation-free I_{D0}. This underestimation affects the extracted V_{th} shift especially for early time of the stress. The smaller time-zero (t_0) is the more accurate data are.

III.3.2 Interface State Density Extraction

To determine the interface state density and its distribution in the band gap, several techniques have been proposed such as the deep-level transient-spectroscopy technique (DLTS), the 1/f noise and the charge pumping method (CP) [18]. CP method is widely used to extract the interface state density in a transistor because of its capability for measurement on small area MOSFET devices. In the context of NBTI, modified CP methods were developed to minimize the time of measurement to prevent the recovery of NBTI [20].

In a conventional CP method the stress is off during the measurement. The source and drain are tied together and weakly reverse-biased (Figure III3) [19]. The gate is driven by a pulse generator from strong inversion to accumulation. The substrate is grounded through a Pico-ammeter to measure the charge pumping current.

The CP current is given by [18]

$$I_{CP} = \overline{D_{it}}\, 2\, q\, f\, A_G\, k_B\, T\, \mathrm{Ln}\left(v_{th} n_i \sqrt{\sigma_e \sigma_h} \sqrt{t_{em,e}\, t_{em,h}}\right) \quad \text{(III.3)}$$

$$t_{em,e} = \frac{|V_{FB} - V_T|}{\Delta V_A} t_f$$

$$t_{em,h} = \frac{|V_{FB} - V_T|}{\Delta V_A} t_r$$

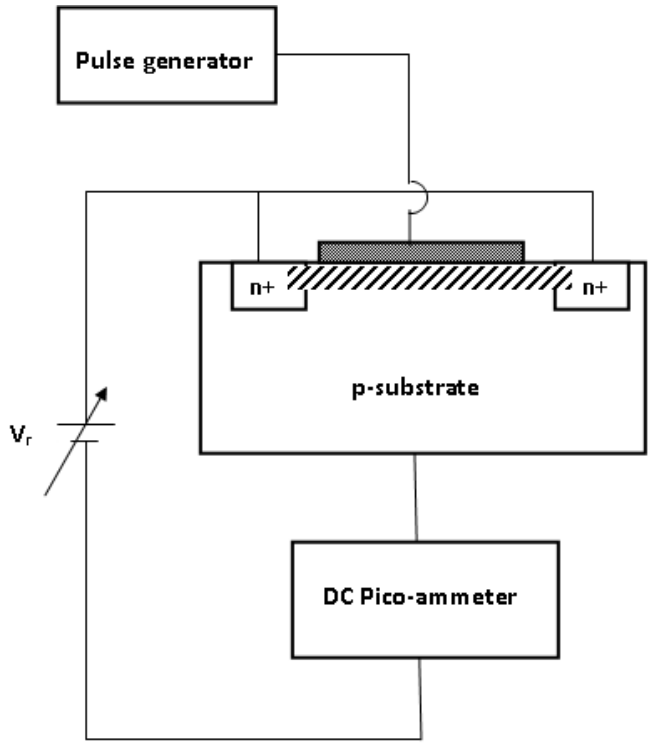

Figure III.3 Conventional charge pumping set-up

where

- D_{it}: the mean density of interface states,
- f: the pulse frequency
- A_G: the gate cross-sectional area
- k_B: Boltzmann constant
- v_{th}: thermal velocity
- σ_e, σ_h: electron and hole capture cross section of a trap respectively

- $t_{em,e}$, $t_{em,h}$: emission time of an electron and a hole respectively

Since the stress in the conventional method is interrupted during measurement and NBTI generated interface traps are believed to recover, the accurate interface trap density is hardly obtained. Many researchers attempt to developed On-The-Fly CP. Ang et al. [20] have developed an ultrafast CP method. At a given interval, a series of positive 100 ns gate pulses of amplitude |Vgs| + 1 V are injected, at periods of 10 μs each. The pulses switched the device between inversion and accumulation repeatedly, inducing a dc surface recombination current measured, with sub-pA resolution, at the source/drain terminal. The pulse wavform is presented in Figure III.4.

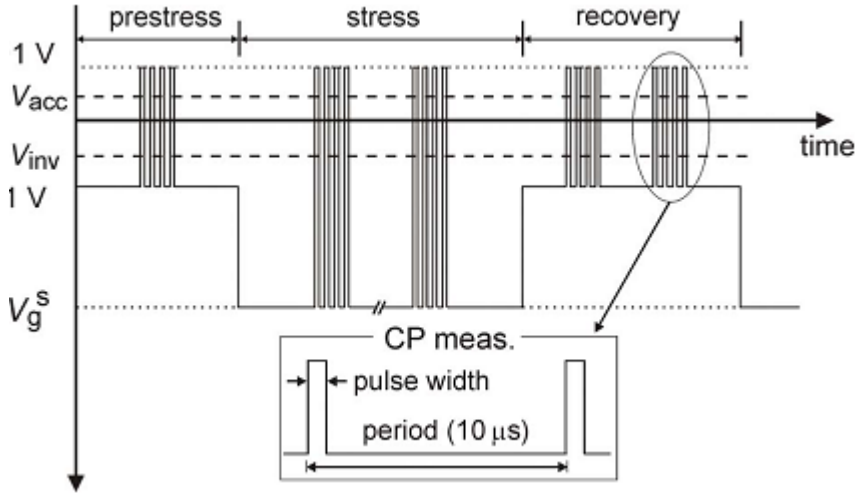

Figure III.4 Ultrafast charge pumping pulse waveform [20]

The charge pumping current is believed to be solely due to interface traps contribution. However Ang et al. [21] give evidence that the CP current is contaminated by the contribution of interfacial oxide traps that participate to the CP recombination process. They attribute the recoverable part of the I_{cp} current to the tunneling of hole from Si substrate to the interfacial oxide traps and the permanent component of I_{cp} to the interface traps contribution. Ang et al. question the accuracy of the CP method for the determination of interface state density [21][22][23][24].

III.4 NBTI KEY FEATURES

NBTI features are the experimental observations related to the degradation behavior that distinguish it from the other reliability wearout mechanisms. Any model of NBTI could be qualified as reliable only if it succeeds in explaining these features. In the following I give some relevant features.

III.4.1 Charge Transport Independence

Unlike the other wearout mechanisms such as hot-carrier injection, oxide breakdown or electromigration where the charge transport activates directly or indirectly the degradation, NBTI is confirmed to be independent from carrier transport because NBTI degradation is observed even if both source and drain are grounded.

III.4.2 Channel Hole Concentration

It is recognized that the presence of holes is essential for NBTI degradation to occur, but whether their concentration has any impact on the NBTI degradation or not is controversial. Huard et al. and many other scientists believe that NBTI does not depend on the channel-hole concentration [11][13-14][26]. However Alam and his group [27-29] always treat NBTI degradation as a hole-concentration dependent phenomenon.

III.4.3 Oxide Field Dependence

It is widely accepted by the NBTI scientist community that NBTI is an oxide field dependent phenomenon rather than gate voltage dependent. Huard et al. [13] investigated the interface traps creation under NBTI degradation for different gate oxide thicknesses, ranging from 2.1 nm to 10 nm-thick while keeping the gate voltage constant.

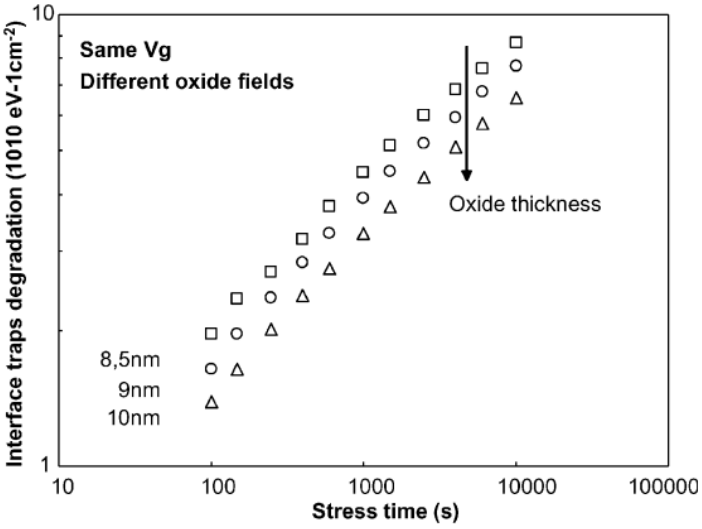

Figure III.5 Interface traps creation for p-MOSFETs for three different oxide thicknesses under similar gate voltage.

When the oxide field is increased, the electrical parameters show a clear increase of their degradation (Figure III.5). These results demonstrate the importance of the oxide field.

The results obtained by Huard et al. are consistent with the results of reference [26] which demonstrated that the oxide field is the driving force of the interface traps creation during NBTI degradation.

The actual gate oxide field dependence of the NBTI damage is still a source of very active research. At this point two empirical models have being adopted [30]:

- Exponential model:

$$\Delta V_T \approx \exp(\gamma F_{ox})$$

- power-law model

$$\Delta V_T \approx F_{ox}^{m}$$

III.4.4 Temperature Dependence

Besides the importance of the oxide field, the NBTI degradation is also activated by temperature. Figure III.6 shows the effect of the temperature on the interface state density.

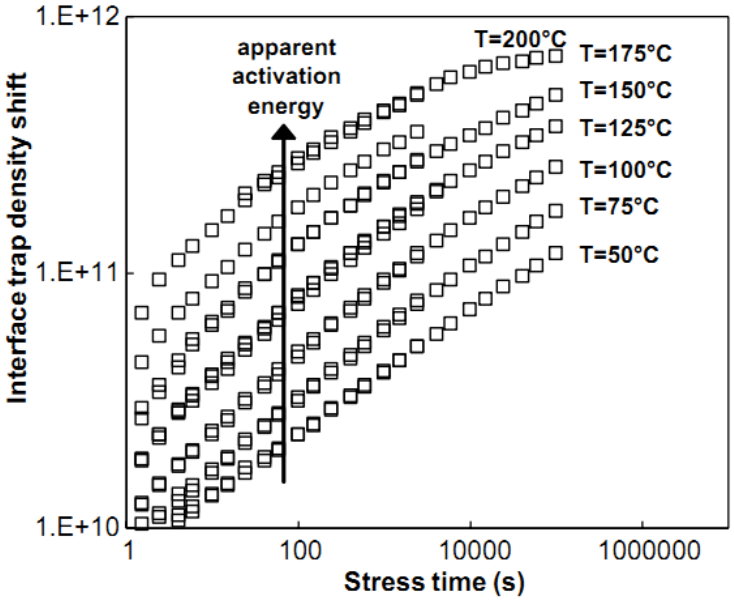

Figure III.6 Interface traps density shift for constant gate voltage stress and for temperature ranging from 50°C to 200°C. [13]

The NBTI temperature dependence is often modeled to follow Arrhenius' law $\exp\left(\frac{-E_a}{KT}\right)$, with activation energy E_a. However, very different values are measured for the activation energy. An activating energy of 0,12 - 0,15 is often given [11].

Many reported data show that the power law exponent increases with temperature [13][25]. This has led some scientists to argue a non-Arrhenius's law.

However, there are other researchers who stand behind the Arrhenius-like behavior attributing the apparent dependence between the time exponent and the temperature to a measurement artifact [28].

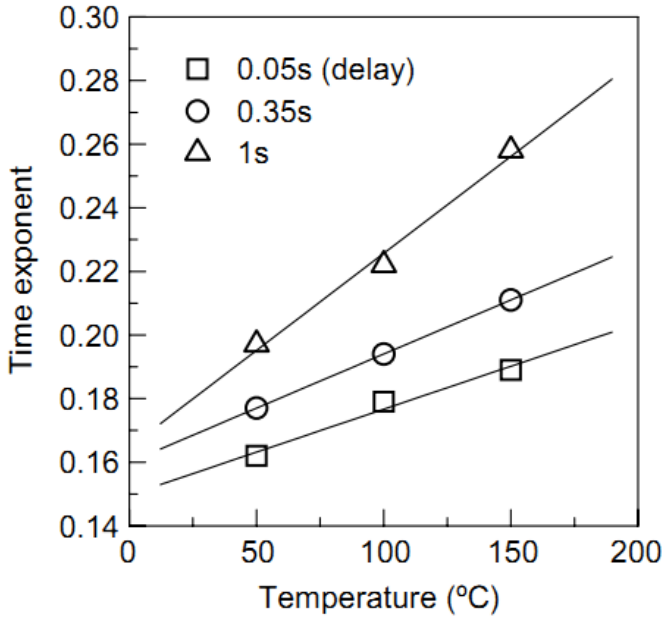

Figure III.7 Temperature dependence of measured NBTI time exponents obtained by conventional measurements with different time delays. [28]

Alam et al. [28] explains the temperature dependence of the time exponent by the inherent measurement delay in the classical measurements. Such delays lead to significant error in determining the true NBTI exponents (see Figure III.7) and therefore any temperature-dependent variation of these parameters cannot be used to reach specific conclusions regarding the mechanics of NBTI degradation. Once the ‘‘zero-delay’’, on-the-fly measurements are used, the temperature dependent degradation curves becomes parallel to each other confirming the Arrhenius like behavior.

III.4.5 The Time Dependence

One of the most important features of NBTI is the slope of the time dependence of the threshold shift when plotted in a log-log scale. The value of this slope called the time exponent (n).

A time dependence of NBTI degradation is clearly observed since as long as the stress lasts more defects are created. It is widely accepted that NBTI follows a power law with

different values of the time exponent as reported in the literature depending on the authors. A value of 0.25 was often given in early experiments, but values less than 0.25 have been also reported [26].

The time exponent n is very sensitive to the measurement time. Varghese et al. show that n = 0.14 for ‘‘no delay’’ measurements and n > 0.14 when there is a delay between stress and measurement. For nitrided oxide n can be as small as 0.10 [11].

Some researchers claim saturation of the degradation i.e. decreasing of the time exponent at latter stage. Again this is explained by the delay inserted during the measurement [28].

It is important to emphasize that caution must be exercised when comparing NBTI time evolution data with different experimental setups and different stressing and testing procedures. These observations may be inconsistent and lead to wrong insights on the physics of the NBTI damage and possible NBTI modeling.

III.4.6 Recovery of NBTI

Rangan et al. [31] were the first to explore the recovery effect using the uninterrupted stress technique. They showed that the recovery mechanism is temperature activated. A device subject to NBTI at room temperature or below will recover nearly to its original state; while a device stressed at a higher temperature displays less recovery.

Recent reports claim logarithmic time (log t) dependence of NBTI recovery based on the ultrafast measurement [35]. Also the recovery of NBTI is reported to be enhanced when it recovers under positive voltage.

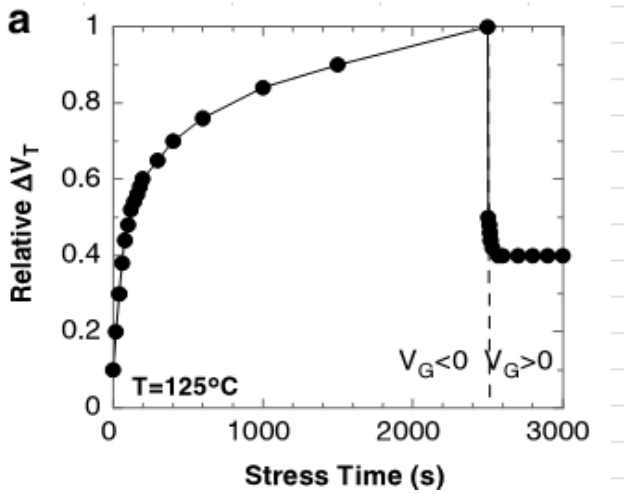

Figure III.8 Relative shifts for ΔV_T versus stress time for NBTI stress and recovery [11].

III.5 CONCLUSION

NBTI is a serious reliability problem and any technological solution adopted in response to industrial downscaling requirements makes the devices more vulnerable to the NBTI degradation. Also, any comprehensive description of the evolution of the NBTI damage must take all the following experimental observations into account:

- Log-like time dependence behavior for earlier stage,
- Power law time dependence for later stage,
- Temperature-dependent power-law exponent for delayed measurement,
- Temperature-independent power-law exponent for undelayed measurement,
- Long relaxation tails of log-like,
- Strong bias sensitivity of the recovery, particularly for positive bias,
- Fast recoverable and slowly recovering/permanent component.

CHAPTER IV

NEGATIVE BIAS TEMPERATURE MODELING

IV.1 INTRODUCTION

Many explanations of the underlying mechanism behind NBTI and modeling attempts have been given over the years. The earliest one is the Reaction Diffusion model first proposed by Jeppson and Svensson [28] thirty years ago and which has been continuously refined since then. Although the Reaction-Diffusion model is able to explain many experimentally observed characteristics of NBTI, the microscopic details are still not well understood. Recently, various alternative models have been put forward contradicting the standard reaction-diffusion model.

The proposed models can be classified into two broad categories:

- Hydrogen-diffusion based models
- Hole-trapping detrapping based models

In this chapter, I will explore an example of each category. The Reaction-Diffusion model is the well-known hydrogen-diffusion based. I will study the model from the earliest (classical) model proposed by Jeppson et al. and ending by highlighting some refinements introduced to the model to meet the experimentally observed behaviors that the model failed to predict.

For the hole-trapping detrapping based model, the two-stage model proposed by Grasser [35] is chosen and discussed.

IV.2 HYDROGEN-DIFFUSION BASED MODELS

The observed increase of the interface trap density during NBTI stress and the role of hydrogen in the passivation of interface traps during the annealing process have led to the conclusion that NBTI is a hydrogen related phenomenon. The substitution of hydrogen by deuterium which is shown to attenuate NBTI degradation [32] is another proof of hydrogen importance for NBTI. For this reason the Reaction-Diffusion RD model has been proposed and it is accepted to be one of the best models describing the mechanism of generation of defects at the interface SiO_2/Si [11].

NBTI, in the context of this model, is regarded to be due to the depassivation and passivation of Si-H (reaction regime) and the behavior of the released hydrogen inside the SiO_2 (diffusion regime).

The model starts from the fact that the interface is passivated by hydrogen so that a large number of Si-H bonds are present in a fresh device (device before NBTI stress) with the chemical form of $Si_3 - Si - H$. It describes the device degradation as a combination of the following phases:

IV.2.1 Reaction Phase

This phase starts just after the application of the stress. The interface traps are generated at the Si-SiO_2 interface. The microscopic mechanism behind the interface trap generation is not clear. The following table summarizes some suggestions:

Reaction	Equation
1	$Si_3 - Si - H + H_2O \leftrightarrow Si_3 \equiv Si \bullet + H_3O^+$
2	$Si_3 - Si - H + h^+ \leftrightarrow Si_3 \equiv Si \bullet + H^+$
3	$Si_3 - Si - H + h^+ \leftrightarrow Si_3 \equiv Si^+ \bullet + \frac{1}{2}H_2$
4	$Si_3 - Si - H + h^+ \leftrightarrow Si_3 \equiv Si^+ \bullet + H^0$
5	$Si_3 - Si - H + H^+(\text{from substrate}) \leftrightarrow Si_3 \equiv Si^+ \bullet + H_2$

Table IV.1 Proposed reactions of the interface trap generation [30].

Figure IV.1 illustrates the mechanism of reaction 5 in table IV.1. A channel hole can tunnel to a Si-H bond during inversion of the p-MOSFET and takes one electron from the covalent bonding thus weakening the Si-H bonds. The hydrogen now can easily be detached from the Si atom and diffuses away leaving a positively charged interface trap behind.

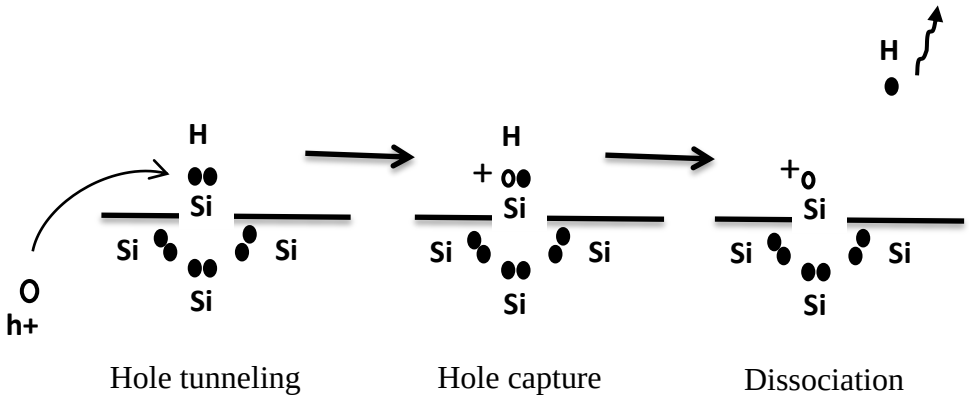

Figure IV.1 The mechanism of Si-H bond breaking according to R-D model and reaction 5

The R–D model describes the rate of generation of interface traps by following equation:

$$\frac{dN_{it}(t)}{dt} = k_f(N_0 - N_{it}) - k_r N_{it} N_H \qquad x = 0 \qquad (IV.1)$$

Where

$x = 0$ denotes the Si–SiO_2 interface and $x > 0$ is (in the oxide) towards the gate,

N_{it} is the number of interface traps at any given instant,

N_0 is the initial number of unbroken Si–H bonds; N_H is the hydrogen concentration,

k_f is the oxide field dependent forward dissociation rate constant,

k_r is the annealing rate constant.

The microscopic details of the trap generation and trap annealing processes that occur within a few Angstrom of the Si/SiO_2 interface are hidden in the constants k_f and k_r.

IV.2.2 Diffusion Phase

The diffusion medium is the amorphous SiO_2. The released hydrogen moves into the oxide by jumping between potential wells. Two approaches here are often used. The first one is to suppose that these potential wells are equal and uniformly distributed across the oxide as shown in Figure IV.2 (Arrhenius approach). In the second, potential wells are not equal and randomly distributed across the oxide as shown in Figure IV.7 (dispersive approach) [25].

IV.2.3 Arrhenius-like Diffusion

Figure IV.2 is a schematic representation of Arrhenius-like diffusion of the hydrogen where the entire potential walls have the same height.

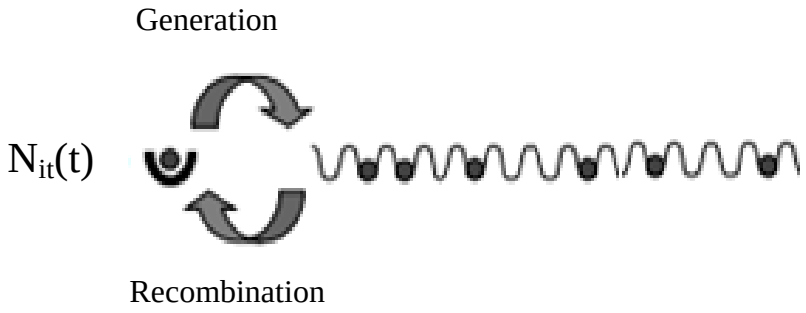

Figure IV.2 Schematic representation of the R-D model principle in the context of Arrhenius behavior [33]

The Arrhenius process is described by the following equations:

$$D_H = D_0 \exp\left(\frac{-E_D}{kT}\right) \quad (IV.2)$$

$$\frac{dN_H}{dt} = D_H\left(\frac{d^2N_H}{dx^2}\right) \quad (IV.3)$$

Where:

D_H is the hydrogen diffusion coefficient,

k is Boltzmann constant,

T is temperature in Kelvin,

E_D is the activation energy of hydrogen diffusion.

For the diffusion phase, the solution of the R-D model can be split up into six different regimes and each regime is characterized by its own time exponent. Figure IV.3 summarize these six regime.

Regime 1: Initially, the N_{it} and N_H values are very low and the reaction is limited only by forward reaction rate k_f and so

$$N_{it} = k_f N_0 t \tag{IV.4}$$

giving a time dependence of n = 1.

Regime 2: After some time, when the amount of hydrogen at the interface is large, the forward reaction reaches quasi-equilibrium with the backward reaction therfor

$$k_f N_0 = k_f N_H(x = 0) N_{it} \tag{IV.5}$$

With N_{it}=N_H we obtained :

$$N_{it} = \sqrt{\frac{k_f N_0}{k_r}} t^0 \tag{IV.6}$$

with a resulting time dependence of n = 0.

As long as the diffusion of hydrogen away from the interface has not reached a large magnitude, there is no further degradation of the interface.

Regime 3: Regime three starts when the diffusion of hydrogen away from the interface starts and acts as a limiting factor for the degradation. In this phase the diffusion front has not reached the polysilicon gate, therefore:

$$\frac{dN_H}{dt} = D_H \left(\frac{d^2 N_H}{dx^2} \right) \tag{IV.7}$$

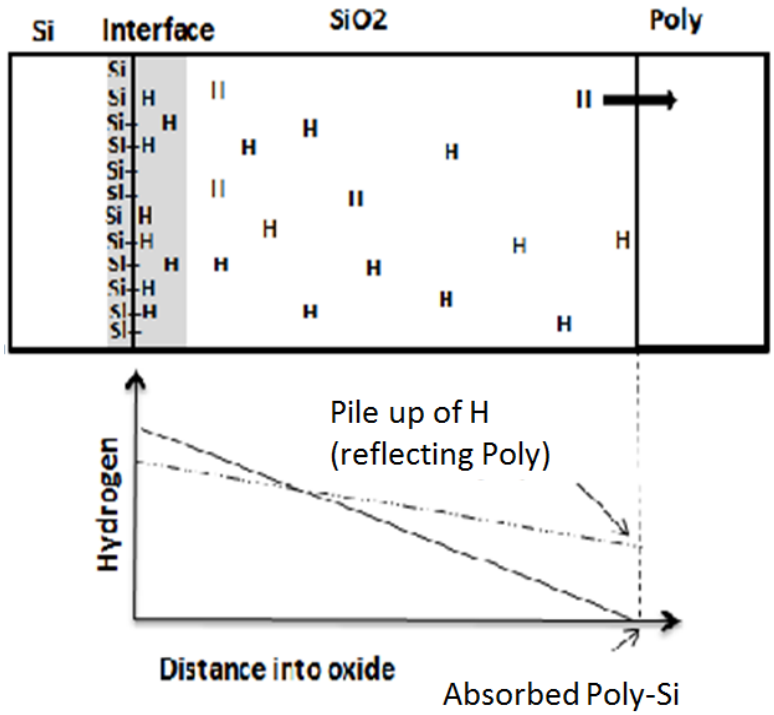

(a)

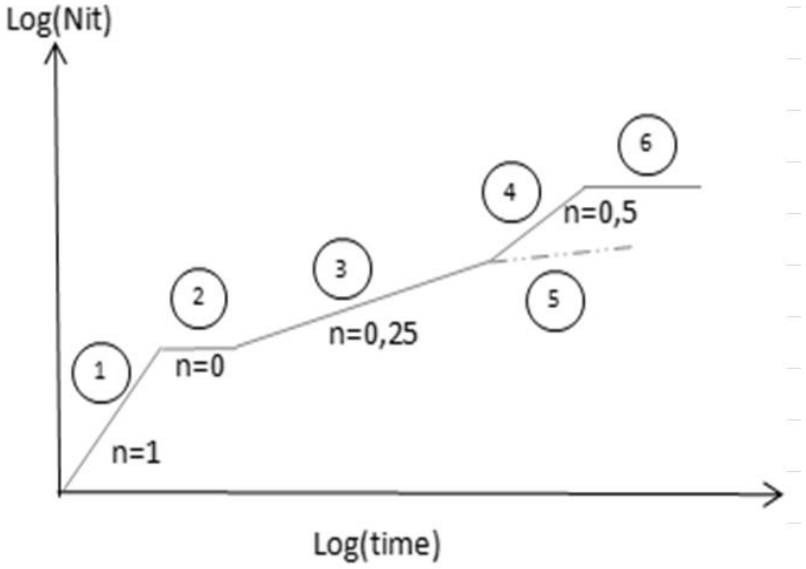

(b)

Figure IV.3 The classical R-D model underlying mechanism representation. a) Hydrogen profile. b) Interface traps generation regimes.

Every dangling Si bond is associated with a free H atom in the oxide. The density of H in the oxide during diffusion can be approximated by a triangular profile [26], with the end front equal to $\sqrt{D_H t}$, thus the interface trap density is given by:

$$N_{it}(t) = \frac{N_H^0}{2}\sqrt{D_H t} \qquad (IV.8)$$

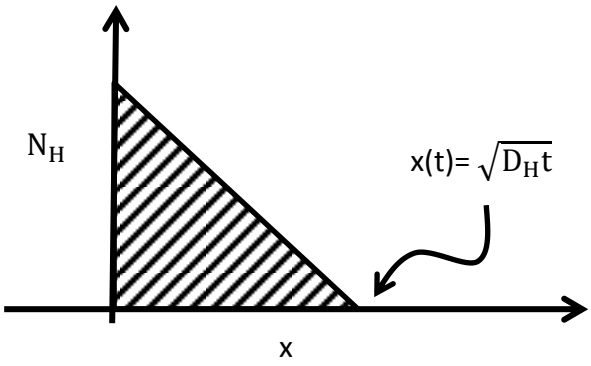

Figure IV.4 The assumed triangular distribution of the released hydrogen atoms in the oxide.

The rate of interface generation is supposed to be constant during this period of the model then the term $\frac{dN_{it}}{dt}$ is neglected and so:

$$N_{it}N_H^0 = \frac{k_f N_0}{k_r} \qquad (IV.9)$$

By combining eq. (IV.9) with eq. (IV.8) we obtained :

$$N_{it}(t) = \sqrt{\frac{k_f N_0}{2k_r}}(D_H t)^{1/4} \qquad (IV.10)$$

which gives the time-exponent (n = 0.25) of NBTI when only H diffusion is taken into account.

Regime 4: When the diffusion end front reaches the polysilicon gate contact the time exponent changes again. In this model it is assumed that the hydrogen species diffuses into the poly-silicon gate with high diffusion constant. That is, the gate electrode acts as an absorber for the diffusing species. For this case a time exponent of n = 0.5 is derived.

Regime 5: If the poly-silicon gate reflects the hydrogen species, they pile up at the oxide gate interface causing the concentration gradient of the hydrogen in the oxide to decrease. As a consequence, the flux of hydrogen species decreases also. The NBTI degradation shows a sign of saturation as illustrated in Figure IV.3-a

Regime 6: When regime 6 is reached, theoretically, all interface bonds N_0 are broken and no further degradation can occur in this model. Therefore the change in N_{it} is zero thus the time exponent n is zero also.

In the previously described R-D model, only H diffusion is considered. However, it is known that atomic H is unstable and it would convert to molecular H_2 after it is released from the Si-SiO_2 interface. Activation energies observed from NBTI measurements support that the dominant diffusing hydrogen species are H_2 [11][13][26]. Therefore, it is worth repeating the derivation of the R-D model by replacing H by H_2.

In the H_2 diffusion-based model, after dissociation of Si−H bonds, the released H atoms transform to the hydrogen molecule according to the following reaction:

$$H + H \leftrightarrow H_2$$

The conversion between H and H_2 would be given by the law of mass action:

$$\frac{N_H(0)^2}{N_{H_2}} = \text{const} \qquad (IV.11)$$

Following the same derivation as for the case of H, we obtain:

$$N_{it}(t) \propto \left[\frac{K_F N_0}{k_r}\right]^{\frac{2}{3}} \left(D_{H_2} t\right)^{\frac{1}{6}} \quad (IV.12)$$

When only the diffusion of H_2 is taken in consideration the time exponent is 1/6. This reflects less degradation because the transformation H-H_2 blocs the diffusion of H atoms allowing them to stay at the interface for more time, then more interface states are passivated.

In addition to the H and H_2 cases, another case is worth considering; when the diffusing species are protons H^+. The NBTI degradation is now drift limited rather than diffusion limited. The profile of the H^+ is approximated to a triangle as shown in Figure IV.5 [26]. The number of interface states is given by:

$$N_{it}(t) = N_H(0)\mu_H E_{ox} t \quad (IV.13)$$

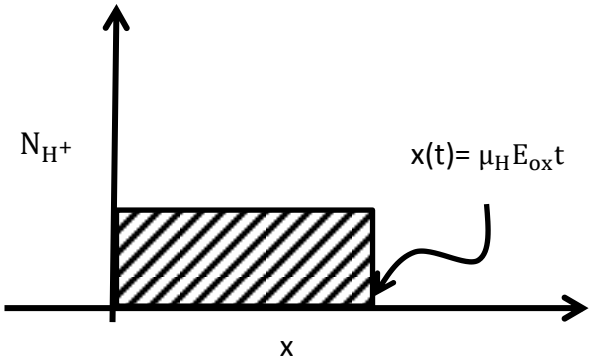

Figure IV.5 The distribution profile of the released H^+ in the oxide.

From eq. (IV.13) and eq. (IV.9), N_{it} is given by:

$$N_{it}(t) = \sqrt{\frac{k_f N_0}{k_r}} (\mu_H E_{ox} t)^{\frac{1}{2}} \quad (IV.14)$$

The time exponent of 1/2 has never been seen in NBTI measurements, leading one to conclude that NBTI degradation through proton transport is unlikely [11] [13] [26].

The following table summarizes the predicted value of the time exponent depending on the diffusing species:

Species	**n**
H^0	0,25
H_2	0,162
H^0 , H_2	0,25-0,165
H^+	0,5
H^0 , H_2, H^+	0,25-0,5

Table IV.2 Value of the time exponent for different diffusing species [34]

The reaction-diffusion model predicts the temperature and the electric-field dependence of NBTI implicitly within the k_f and k_r coefficients. The oxide-field dependence (exponential dependence) is included in the k_f term and the temperature dependence of the degradation is incorporated through the activation energies of k_f , k_r and D_H in the form of Arrhenius activation.

In the recovery phase, when the stress is turned off, the forward reaction coefficient k_f is zero and only the backward reaction takes place. The quantity of hydrogen available at the interface rapidly repassivates the dangling bonds. Afterward the repassivation is diffusion controlled. It is governed by the following equation [4]:

$$N_{it} = N_{it}^{(0)}\left(1 - (\xi t/t_0)^{1/2}/(1 + t/t_0)^{1/2}\right) \ (t > 0) \qquad (IV.15)$$

Where

t_0 time when the stress is stopped,
$Nit^{(0)}$ the number of traps generated at t_0,
ζ= ½ for one sided diffusion.

IV.2.4 Dispersive Transport

The Reaction-diffusion model described above assumes hydrogen species to diffuse into the oxide according to an Arrhenius-like activated transport. If we assume k_f, k_r and D_H to be given as follows [28]:

$$k_f = k_{f0}\exp(-E_F/kT),$$

$$k_r = k_{r0}\exp(-E_R/kT),$$

$$D_H = D_0\exp(-E_D/kT),$$

where

E_F is the activation energy of the forward reaction rate,
E_R is the activation energy of the backward reaction rate and
E_D is the activation energy of the hydrogen diffusion.

Then the interface state density will be given by [28]:

$$N_{it}(t) \propto \left(\frac{k_{f0}N_0}{k_{r0}}\right)^m D_0^n e^{-\frac{m(E_F-E_R)+nE_D}{kT}} t^n \qquad (IV.16)$$

Where n, m depends on the diffusion species.

Therefore for the Arrhenius transport (Diffusion nature) , the threshold shift curves plotted in a log-log scale at various temperatures as a function of time should be parallel to each other (n is independent of temperature). In contrast, the obtained curves show that the time exponent n varies with temperature (Figure IV.6). This is why many scientists invoke the non-Arrhenius and dispersive nature of NBTI degradation.

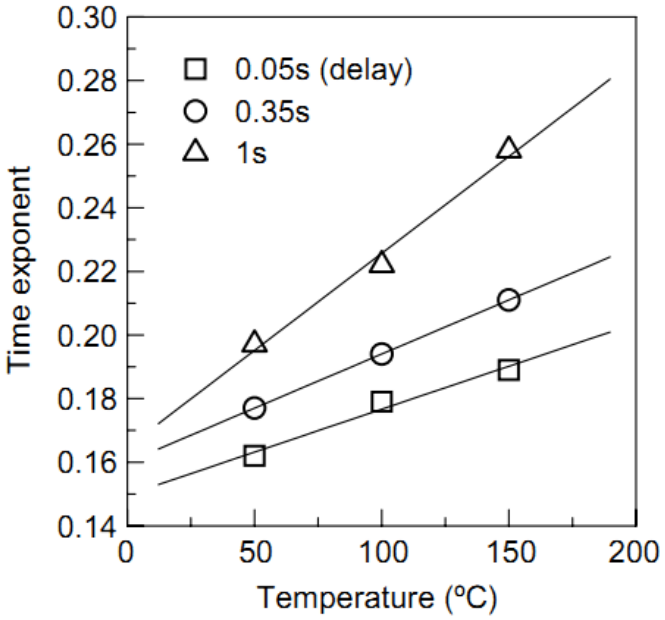

Figure IV.6 Temperature dependence of measured NBTI time exponent.[28]

Figure IV.7 is a schematic illustration of dispersive transport where the dielectric contains hydrogen traps of different energy. The trapping probability at each trap is the same. But for de-trapping it is different; deeper traps present a higher barrier than the shallow ones. Transport hydrogen species spend most of their lifetime in the deeper traps, which thus control their transport properties.

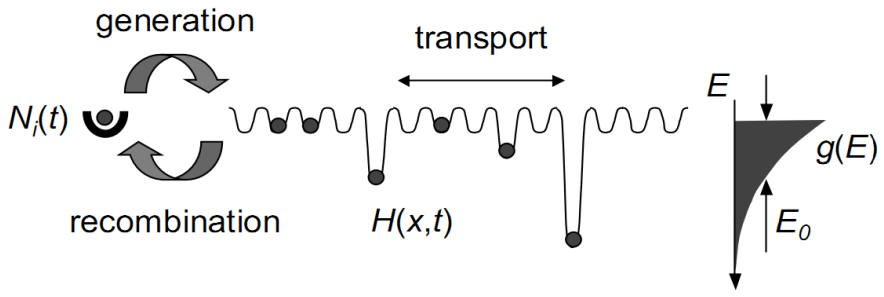

Figure IV.7 Schematic representation of the dispersive transport of hydrogen species.

N_{it} is then given by [33]

$$N_{it}(t) \propto \left(\frac{k_{f0}N_0}{k_{r0}}\right)^m \left(\frac{D_{H0}}{\upsilon}\right)^n e^{-\frac{m(E_F-E_R)}{kT}} (\upsilon t)^{n(1-\alpha)} \qquad (IV.17)$$

Where

υ is the hopping frequency of hydrogen

α is the dispersive parameter. It can vary between 0 (conventional transport) and 1 (strongly dispersive transport).

IV.3 HOLE-TRAPPING DETRAPPING BASED MODEL

In spite of its success in describing many experimental results of NBTI degradation, R-D model faces growing criticism from many research labs. It is especially pointed out that:

- Generated interface traps do not show any recovery,
- The logarithmic dependence on time of the recovery,
- The cyclic behavior of the NBTI stated by Ang et al.

IV.3.1 Two Stage Model

A more elaborated multi-mechanism explanation is the two stage model proposed by T. Grasser, et al. [35]. In this theory the precursor for the phenomenon is a neutral interfacial oxygen vacancy, which upon the capture of a hole, creates a positive defect called an E'_γ center. Next, the emission of the captured hole (electron capture) neutralizes the defect at which point the structure can either relax back to the original oxygen vacancy precursor, or re-capture a hole and return to the E'_γ state. This is the mechanism believed to account for the rapid charging and recovery dynamics observed in NBTI. As for the second mechanism, the E'_γ center can interact with the hydrogen passivating a neighboring silicon dangling bond at the interface. Lenahen and Campell [36] demonstrate that it is energetically favorable for the hydrogen to migrate to the E'_γ center leaving behind an interface state whose charge will depend on the position of the Fermi-level.

Figure III.8 illustrates the principal of the two stage model proposed by T. Grassor.

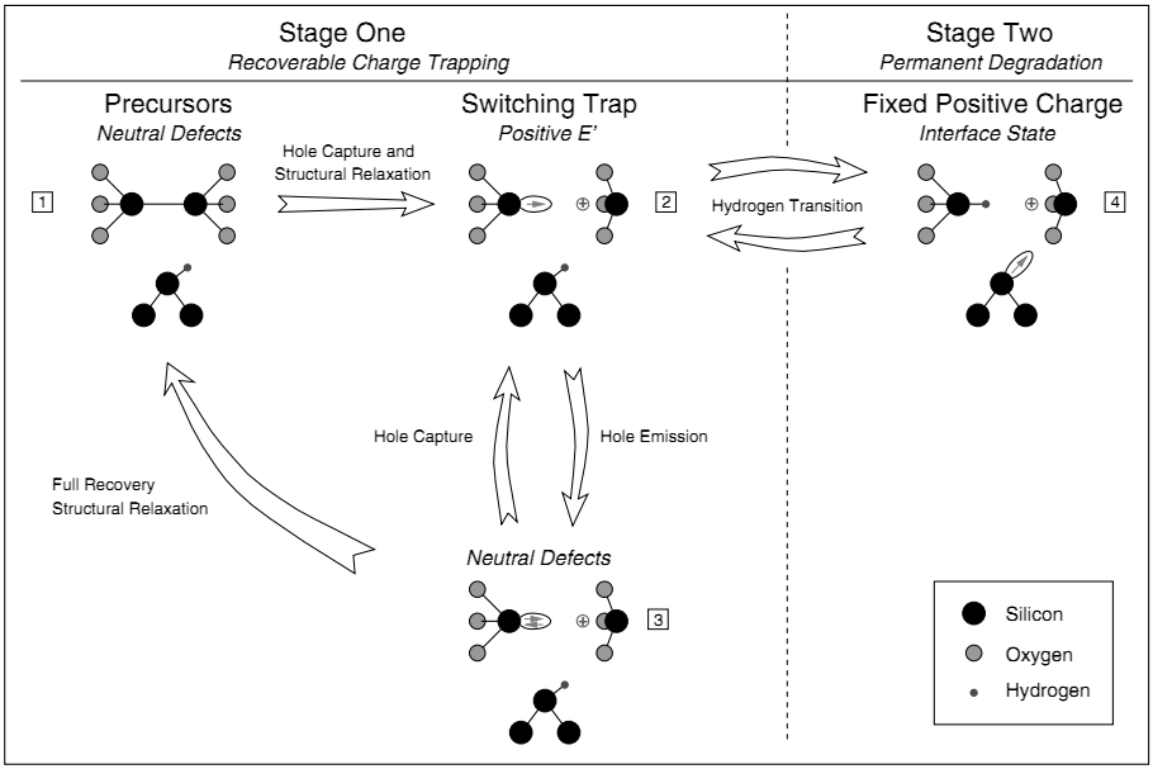

Figure IV.8 Two stage model principle. Stage one is based on the hole-trapping detrapping model for switching traps. Stage two illustrates a hydrogen transitions which results in the creation of an interface state.[36]

By considering a trap level E_T located at a distance x away from the interface as shown in Figure IV.9, the hole capture and emission rates are then approximately given by [36]:

$$K_p^c = p\, v_p^{th} \sigma_p e^{-x/x_{p,0}} e^{-\beta \Delta E}\, \theta\left(E_{VT}\, e^{-\beta E_{VT}},\, 1\right) e^{F^2/F_c^2} \qquad (IV.18)$$

$$K_p^e = p\, v_p^{th} \sigma_p e^{-x/x_{p,0}} e^{-\beta \Delta E}\, \theta\left(E_{VT}\, e^{-\beta E_{VF}},\, e^{-\beta E_{TF}}\right) \qquad (IV.19)$$

while the corresponding rates for electrons is:

$$K_n^c = n\, v_n^{th} \sigma_n e^{-x/x_{n,0}} e^{-\beta \Delta E}\, \theta\left(E_{TC},\, e^{-\beta E_{TC}},\, 1\right) \qquad (IV.20)$$

$$K_n^e = n\, v_n^{th} \sigma_n e^{-x/x_{n,0}} e^{-\beta \Delta E}\, \theta\left(E_{TC},\, e^{-\beta E_{FC}}\, ,\, e^{\beta E_{TF}}\right) \qquad (IV.21)$$

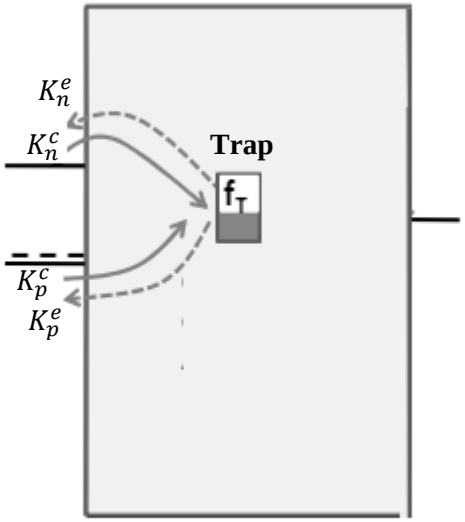

Figure IV.9 Carrier capture and emission coefficients of an oxide trap at energy level E_T.

where

p and n are the hole and electron concentrations in the channel,

v^{th}_p and v^{th}_n are their thermal velocities,

σ_p and σ_n are their capture cross sections,

E_F is the Fermi-level in the channel, E_V and E_C are the valence and conduction bands directly at the interface (classical approximation),

ΔE is the multiphonon emission barrier,

Fc is the reference field for the multiphonon-field- assisted tunneling mechanism,

$x_{n,0}$ = 0.8 A for electrons; and $x_{p,0}$ =0.5 A for holes.

θ is the auxiliary function. It is used to account for the fact that thermal activation is required for hole capture into a trap below E_V while capture in a trap above E_V proceeds without activation, and vice-versa for electrons.

$$\theta(E_{swich}, a, b) = \begin{cases} a & E_{swich} \geq 0 \\ b & E_{swich} \geq 0 \end{cases}$$

a) First stage

Initially the defects before stress are in state 1 (Figure IV.8). The trap energy lies at E_T has a multiphonon emission (MPE) barrier of ΔE_B, and a multiphonon-field-assisted tunneling (MPFAT) reference field F_c.

After the application of the stress, defects starts to transform from state "1" to state "2" by capturing a hole from the inversion layer with a rate of $f_1 k_{12}$, where f_1 is the probability of the defects to be in state "1" and k_{12} is the rate of transformation from state "1" to "2".

Being in state "2" (charged E'γ center) the defects can transform to state "3" with a rate of $f_2 k_{23}$ or pass to state "4" by capturing a hydrogen from the Si-H bonds.

Defects in state "3" (neutral E'γ) can transform back to state "2" by emitting the captured hole with a rate of $f_3 k_{32}$ or totally anneal and returns back to state "1"

In general, the rate equations describing the transitions between the three states are given by:

$$\frac{\partial f_1}{\partial t} = -f_1 k_{12} + f_3 k_{31} \qquad (IV.22)$$

$$\frac{\partial f_2}{\partial t} = +f_1 k_{12} - f_2 k_{23} + f_3 k_{32} \qquad (IV.23)$$

$$\frac{\partial f_3}{\partial t} = +f_2 k_{23} - f_3 k_{32} + f_3 k_{31} \qquad (IV.24)$$

f_1, f_2 and f_3 are the probability of the trap to be in state 1, 2, and 3 respectively.

The rate of transition between states 1 to 2 is given by:

$$k_{12} = k_p^c(E_T, \Delta E_B, F_C) + k_n^e(E_T, \Delta E_B, F_C) \qquad (IV.25)$$

In a similar way, the transition from state 2 to state 3 are described by:

$$k_{23} = k_p^e(E'_T, \Delta E_c, 0) + k_n^c(E'_T, \Delta E_c, 0) \qquad (IV.26)$$

$$k_{32} = k_p^c\left(E'_T,\ \Delta E_c, 0\right) + k_n^e\left(E'_T,\ \Delta E_c, 0\right) \quad \text{(IV. 27)}$$

$$K_{31} = v\exp(-\beta\Delta E_A) \quad \text{(IV. 28)}$$

b) Second stage

Stage two of the model deals with the interface traps generation. By the end of stage one created interfacial E'γ triggers the hydrogen dissociation from the Si-H bonds.

The transition rates between state 2 and 4 are modeled as follows:

$$K_{24} = v\exp(-\beta(\Delta E_D - E_2 - \gamma F) \quad \text{(IV. 29)}$$

$$K_{42} = v\exp(-\beta(\Delta E_D - E_4 + \gamma F) \quad \text{(IV.30)}$$

IV.3.2 Threshold Voltage Shift Expression

By determination of the oxide charge Q_{ox} and the interface charge Q_{it}, the threshold shift is given by

$$\Delta V_{th}(t) = -\frac{\Delta Q_{ox}(t) + \Delta Q_{it}}{C_{ox}} \quad \text{(IV. 31)}$$

In the context of the Two stage model Q_{ox} is the density in the bulk of E' centers that are in state "2"

$$Q_{ox}(t) = q\frac{1-x}{t_{ox}}\langle f_2(t)\rangle \quad \text{(IV. 32)}$$

and

$$\Delta Q_{ox}(t) = Q_{ox}(t) - Q_{ox}(0) \quad \text{(IV.33)}$$

The interface trap charge Q_{it} is given by the average of the probability of having depassivated dangling bonds (state 4) times the probability that the created electrical level of the donor-like defect is unoccupied:

$$Q_{it} = q\langle f_4(1 - f_{it})\rangle \qquad (IV.34)$$

IV.4 CONCLUSION

In this chapter, I have investigated two models for the negative bias temperature: the classical reaction-diffusion model and the two stage model proposed by T.Grassor. The first model is a hydrogen-diffusion based model whereas the latter is a hole-trapping detrapping based model.

None of them is able to reproduce all the experimental signatures of the NBTI. This is explained by the fact that NBTI is heavily dependent on the oxide process and that the experimental results themselves do not reflect the intrinsic behavior of the NBTI degradation because of the recovery effect which cannot be eliminated during measurements.

CHAPTER V

THE PROPOSED NBTI MODEL FOR PURE SiO_2

V.1 INTRODUCTION

It is widely recognized that the negative bias temperature instability can be split into two components: a recoverable component on the top of a slowly recovering or even permanent component. But disagreements between authors appeared as to the nature of these components. Some researchers attribute the recoverable component to the stress-induced interface traps and the permanent one to the bulk defects generated during the stress phase, while others claim the recoverable part to be due the hole trap neutralization and the permanent part to the interface traps. A third opinion suggests that only one degradation mechanism is behind the two components.

In this chapter, I propose a model for the negative bias temperature instability for pure SiO_2 that can better explain both the recoverable and the permanent components.

V.2 MECHANISM BEHIND NBTI IN PURE SiO_2

Although accepted to enhance NBTI, nitrogen effect on NBTI degradation is still under debate. Many studies were dedicated to the study of the nitrogen effect on NBTI by comparing the NBTI evolution in pure SiO_2 and nitrided oxide of different nitrogen

concentration. The common conclusion, whether explicitly or implicitly expressed, between these studies is that for pure SiO_2 only one mechanism is taking place.

To get more insight on this conclusion, I choose to present three arguments from different research groups:

1- Ang et al. were interested by the temperature dependence of NBTI for ultra-thin gate oxide.
2- Campell and Lenahan focused on the electron spin resonance study of NBTI
3- Huard et al. dealt with the recovery behavior of NBTI of different oxide processing

The main reason for choosing these three groups is that they have studied NBTI degradation from different views, giving, therefore, a better insight into the mechanisms behind NBTI degradation.

First, Ang et al. in their paper "Evidence of Two Distinct Degradation Mechanisms From Temperature Dependence" [37] tackle the NBTI via a detailed experimental study on the temperature dependence of NBTI-induced degradation of various oxide processing of a p-MOSFET over a very wide range of temperature (−80°C to 160°C).

Figure V.1 shows the Arrhenius plot for Device A and B (oxinitrided oxide) and device C (pure SiO_2). Many salient features can be drawn out from this experiment:

- The pure SiO_2 (open triangle in figure V.1) exhibits a consistent Arrhenius behavior with a typical activation energy of ~0.27 eV. This indicates that only one mechanism is governing the degradation. The relatively high activation energy (of ~0.27 eV) implies that positive trap generated via this mechanism is limited by the transport of hydrogen species released from the dissociation of Si–H bonds.

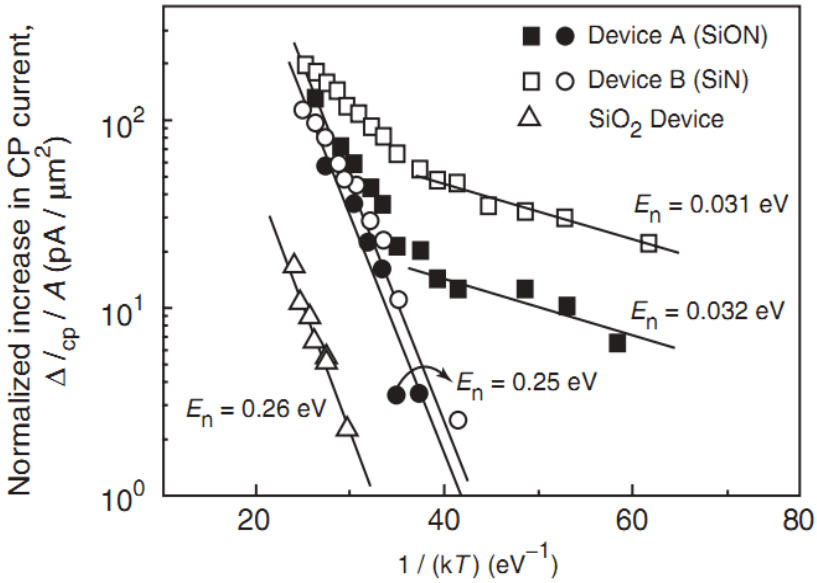

Figure V.1 Arrhenius plots for NBTI stress-induced interface state (Nit) generation in oxinitrided oxides (devices A and B) and in pure SiO_2 [38]

- In the case of oxinitrided oxide device (open circle and square in figure V.1), non-Arrhenius behavior is observed. This implies that a single defect generation mechanism cannot adequately describe the evolution of NBTI for this type of oxides.
- The activation energy observed at low temperatures for devices A and B is very small (~0.037eV). By extrapolating the Arrhenius plot to the high-temperature regime (dashed line) and subtracting it from the measured curve, the Arrhenius plot denoted by filled circles and squares is obtained. The obtained E_a of 0.24 eV falls in the 0.2–0.3 eV range previously reported for conventional SiO_2 gate devices.

From the above results, Ang et al. concluded that increased NBTI of nitrided gate oxide is a consequence of the superposition of a new degradation mechanism, weakly dependent on temperature, onto the classical mechanism responsible for the NBTI of pure SiO_2 gate devices.

The second insight is given by Campell and Lenahan [6] [36] [39]. They studied the defect involved in NBTI degradation at an atomic scale by combining dc gate-controlled diode

measurements of interface-state density with very sensitive electrically detected magnetic-resonance measurements called spin-dependent recombination (SDR). In SDR, the device is placed in a large slowly varying dc magnetic field that partially aligns the spins of the conduction electrons, the holes, and the deep level defects. If a deep level defect and a charge carrier have the same spin orientation, the Pauli Exclusion Principle forbids charge capture by the deep level. When a paramagnetic deep level's electron spin resonance condition is satisfied, the defect's electron spins are "flipped." Flipping the spins increases the probability of opposite spin orientations between deep level defects and charge carriers, thus increasing the recombination current. This increase in recombination current is what is measured in SDR.

Figure V.2 shows the results of SDR of a pMOSFET device with a pure SiO_2 before and after a NBTI stress.

Electrically active defects are distinguished by a parametric value called g. It were observed two strong signals at g = 2.0057 ± 0.0003 and g = 2.0031 ±0.0003. The g = 2.0057 signal is attributed to P_{b0} centers and the g = 2.0031 signal to P_{b1} centers. No E' center (g = 2.0007) generation after the stress is observed.

There is a correlation between NBTI-induced interface state generation and the generation of P_{b0} and P_{b1} interfacial silicon dangling bonds. P_{b0} and P_{b1} are both silicon dangling-bond defects in which the central silicon atom is back-bonded to three other silicon atoms precisely at the Si/SiO_2 interface.

Campell et al. concluded that NBTI in pure SiO_2-based device is dominated by the generation of these P_{b0} and P_{b1} interface defects, therefore the dissociation of the Si-H bonds at the interface.

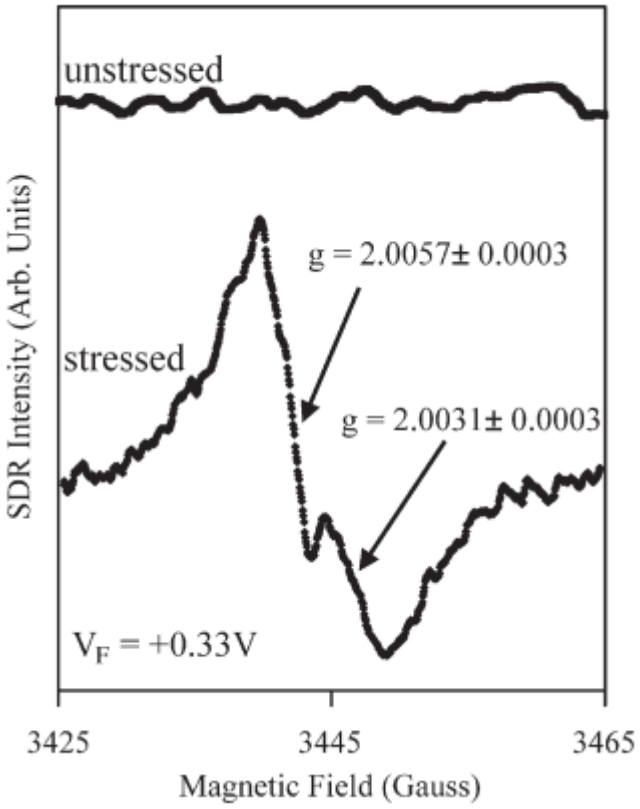

Figure V.2 SDR results of a pure SIO2 pMOSFET device before and after and NBTI stress of −5.7 V at 140°C for 250 000

In the case of nitrided oxide, they demonstrated that the dominating NBTI-induced defect is fundamentally different from those observed in pure-SiO_2-based devices. They defined the defects as silicon dangling bonds, in which the central silicon is back-bonded to a nitrogen atom, which is called K center. They also demonstrated that a very significant fraction of these K centers can behave as interface traps.

The third insight is brought from the work of Huard et al. [13][14][32]. In order to determine the nature of the defects in nitrided oxide, they apply a positive gate bias consecutively to a negative bias stress. The experiment showed a small effect on pure oxide but a large effect for the nitrided oxide. Moreover, the nitrided oxide and pure-SiO_2 both relax down to a similar threshold voltage value. The non-dependence of the NBTI recovery on the positive bias suggests the defects behind NBTI in pure SiO_2 are neutral. Furthermore, the introduction of nitrogen does not have any effect on the degradation

mechanism observed in pure SiO_2, but adds a new mechanism which Huard et al. attributed to the hole traps creation.

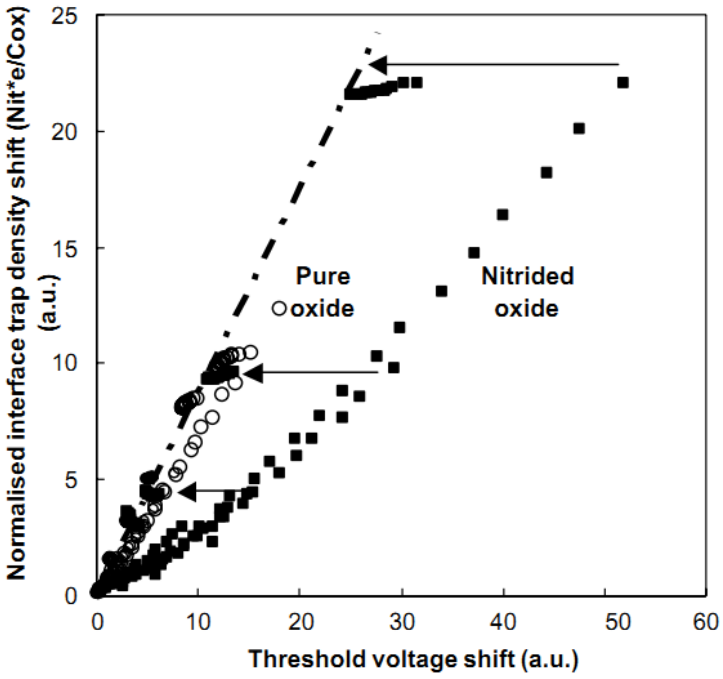

Figure V.3 Correlation plot between the threshold voltage shifts and the normalized interface trap density shift for a pure oxide device (open symbols) and a nitrided oxide device.

From the work of the three groups presented here and other groups, I can summarize the NBTI degradation according to the following framework:

- In pure SiO_2 based devices only one mechanism governs the NBTI degradation which is widely explained through the modified Reaction-Diffusion model.
- Introduction of nitrogen effect is controversial. It:
  - Does not affect the classical SiO_2 mechanism and introduce a new degradation which is explained by hole-trapping and detrapping by nitrogen related defects,
  - Suppresses the classical SiO_2 degradation and introduce a new degradation related to nitrogen defects which can act as interface states and bulk oxide traps,

- Affects the classical model by:
  - Enhancing the degradation i.e. the diffusion of the hydrogen spices in the context of Reaction-Diffusion model
  - Inhibiting the recovery of the classical mechanism. Only the new introduced nitrogen related defects recover.

V.3 NBTI MODEL FOR THE PURE SiO_2

In this section, I propose a model for the NBTI in pure SiO_2. The proposed model is a modification of the well-known Reaction-Diffusion model discussed in chapter IV. The proposed model combines two models already proposed by Küflüoglu [41] et al. and Kumar et al. [43].

Although the nature of NBTI degradation mechanism is controversial , in my proposed model I describe NBTI in pure SiO_2 to be:

- Caused only by one mechanism (Ang et al).,
- Related to P_b center creation (Campell et al), and
- Limited by neutral species (Huard et al)

One model that can reconcile with these three facts is the Reaction-Diffusion model. Under this R-D framework, called the classical R-D, the model succeeded in explaining several experimental observations such as: the time-exponents, the activation energies, the relaxation dynamics of degradation, the frequency dependence under AC stress and the quasi-saturation of NBTI [27][28][29].

In spite of all this success, the classical R-D model which has been presented in the previous chapter still suffers from many weaknesses some of which are listed below:

- Initial higher slope (within 10 s) [41],
- Predicting a slower initial recovery, with most of the subsequent recovery taking place over about three decades of time [21],
- Prediction of a 50% reduction in V_{th} when the relaxation time is equal to the stress time with is not consistent with experiments,

- Fit with experimental data is not very accurate, particularly during the initial phase of the recovery.

The proposed model modifies two assumptions used in deriving the classical model:

1- The transformation of released H atoms to molecular hydrogen (H_2) and the subsequent diffusion of the latter is supposed to be instantaneous
2- The oxide thickness is supposed to be infinity

For the first assumption, theoretical calculations [28] suggest that atomic H is unstable and converts into molecular H_2 after it is released from the Si/oxide interface. The classical R–D model assumes that this conversion is extremely fast, and H is consumed totally at the interface to generate H_2. However, this assumption may not be realistic. Instead, It is most probable that while the atomic H atoms diffuse into the oxide, they convert to H_2. The backward reaction is possible, that is, the H_2 can dissociate into H atoms.

The second assumption is not accurate in practical cases. Assuming the oxide physical thickness to be around 1–2 nm (typical of today's advanced CMOS technologies), and considering, for example, that the diffusivity of molecular hydrogen H_2 in SiO_2 is around $1.32\ 10^2\ nm^2/sec$, it is easy to estimate that the H_2 profile will reach the SiO_2/poly interface within 7.5 ms. This time is much shorter than the stress time typically used during NBTI experiments. This means that for typical NBTI stress conditions, most of the H_2 diffusion should be taking place in the polysilicon gate.

The proposed model aims to improve the classical R-D model to remove some of its mentioned weaknesses.

V.4 MATHEMATICAL FORMULATION OF THE MODEL

The proposed model follows the same patterns as the classical R-D and is, therefore, fragmented into two regimes: the reaction regime and the diffusion-limited regime. Besides, the latter regime has two sub-regimes: the diffusion into the oxide and the diffusion into the polysilicon.

V.4.1 Reaction Phase

Under a negative bias and at a specific temperature, holes pile up at the silicon-dioxide interface of a pMOSFET transistor. These holes can tunnel and be captured by the Si-H bonds causing the bond to be weaker. Hydrogen atom is detached as a result of thermal vibrations according to the following reaction:

$$Si_3 - Si - H + h \rightleftharpoons Si_3 \equiv Si \bullet + H^0 \qquad (V.1)$$

The remaining Si dangling bond (Si•) acts as a donor-like interface trap.

The H released from the bond can diffuse away from the Si/SiO_2 interface or anneal an existing trap. The interface trap density N_{IT} increases with the net rate given by:

$$\frac{dN_{it}(t)}{dt} = k_f(N_0 - N_{it}) - k_r N_{it} N_H^0 \qquad (V.2)$$

Where N_{it} is the number of interface traps at any given instant,

N_0 is the initial number of unbroken Si–H bonds,

N_H^0 is the hydrogen concentration at the interface,

k_F is the oxide field dependent forward dissociation rate constant, and

k_r is the annealing rate constant,

V.4.2 Diffusion into the Oxide

The released H atoms from the Si-H bonds will diffuse away from the interface into the oxide and convert to H_2. the mutual conversation between H and H_2 is governed by the following equation:

$$H + H \leftrightarrow H_2 \qquad (V.3)$$

The time rate of change of H into H_2 is given by:

$$\frac{dN_H}{dt} = -2(K_{H1} N_H^2 - K_{H_2} N_{H_2}) \qquad (V.4.a)$$

Similarly the time rate of transformation of H_2 to H is:

$$\frac{dN_{H_2}}{dt} = K_{H1}N_H^2 - K_{H_2}N_{H_2} \qquad (V.4.b)$$

where k_{H1} and k_{H2} are the generation and dissociation rates for H_2 molecules.

Since the hydrogen species pass just a very short time in the amorphous oxide, the dispersive effect can be neglected and the Arrhenius behavior of the NBTI degradation is not far from being realistic. For that reason the diffusion of hydrogen atoms in the oxide is modeled by:

$$\frac{dN_H}{dt} = D_{Hox}\left(\frac{d^2N_H}{dx^2}\right) \qquad (V.5)$$

And for the H_2 diffusion in the oxide:

$$\frac{dN_{H2}}{dt} = D_{H2ox}\left(\frac{d^2N_{H2}}{dx^2}\right) \qquad (V.6)$$

D_{Hox} and D_{H2ox} are the diffusion coefficients of H and H_2 in the oxide respectively.

Figure V.4.a schematically represents the H and H_2 profile during the oxide-diffusion regime

V.4.3 Diffusion into the Polysilicon Gate

Once the front of the hydrogen species reach the oxide-gate interface, and assuming continuity between oxide and polysilicon and no consumption nor production of hydrogen species occurs at the interface, the hydrogen species enter to a new medium with different characteristics. The atomic hydrogen H^0 is supposed to be consumed in the oxide and transformed to molecular hydrogen H_2 before reaching the oxide-gate interface. H_2 diffusing equation into the polysilicon is given by:

$$\frac{dN_{H2}}{dt} = D_p\left(\frac{d^2N_{H2}}{dx^2}\right) \qquad (V.7)$$

where D_p is the diffusion coefficient of the H_2 molecule in the polysilicon gate.

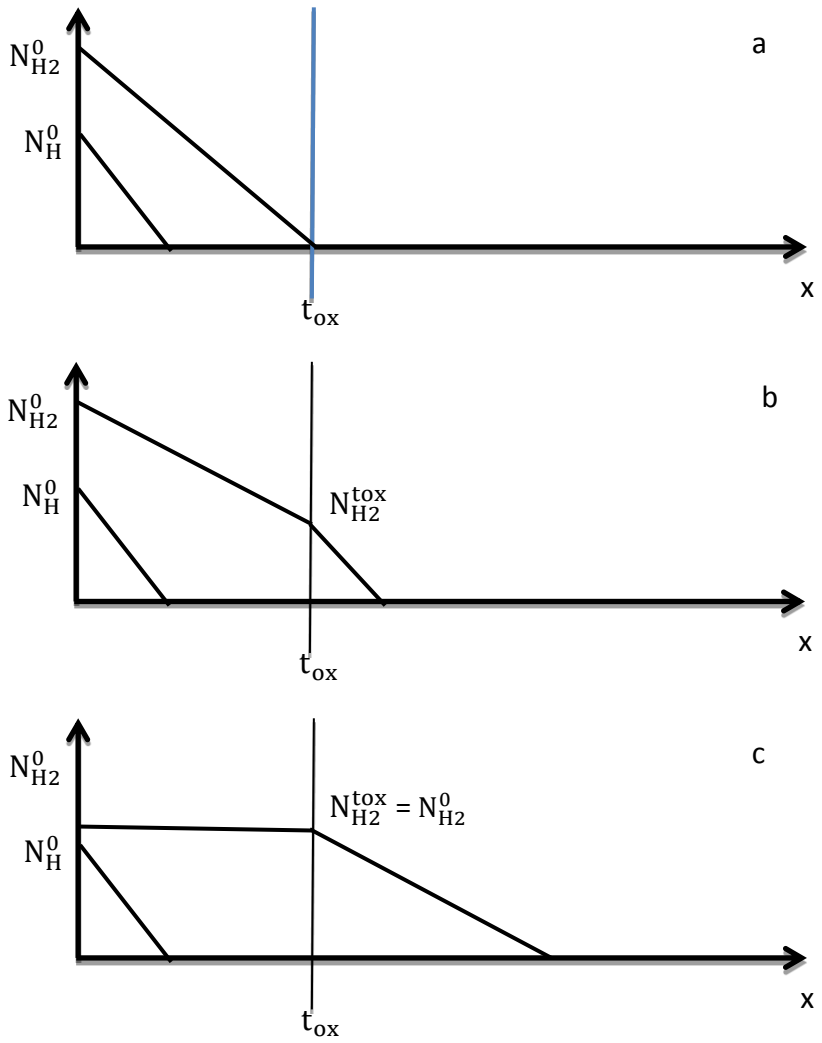

Figure V.4 Schematic representation of the Hydrogen species profile during the stress phase.

The key feature of the proposed model lies in the different nature of the diffusing medium. According to the results of [40], the diffusing coefficient of H_2 in polysilicon is smaller

than in SiO_2. As consequence this difference, H_2 molecules move slower in the ploy-silicon then they do in the oxide. Hence H_2 start to pile up in the oxide while continuing to diffuse in the poly-silicon as illustrated in Figure V.4.b.

Figure V.4.c depicts the hydrogen profile when the gradient of the H_2 in the oxide is zero because the produced hydrogen at the Si-SiO_2 interface moves faster in the oxide than in the poly. This stage determines the long time NBTI degradation.

V.4.4 Recovery Phase

At the time when the stress is off, Hydrogen atoms in the oxide bulk diffuse back to the Si-SiO_2 interface. At early time the hydrogen species in the oxide bulk diffuse back to the interface while the hydrogen molecules continue to diffuse away from the interface. The hydrogen profile is as depicted in Fig V.5.a.

Because of the different diffusing coefficients, the hydrogen species in the oxide diffuse back rapidly due to their higher diffusivity coefficient. The subsequent recovery is limited by the back diffusion of hydrogen molecules in the poly silicon oxide (figure V.5.b).

The complex nature of the dynamics in the proposed model does not permit understanding the time-dependence of NBTI through analytical solution. Therefore, numerical solutions are needed to evaluate the effects of $H - H_2$ transformations and H_2 diffusion in the polysilicon.

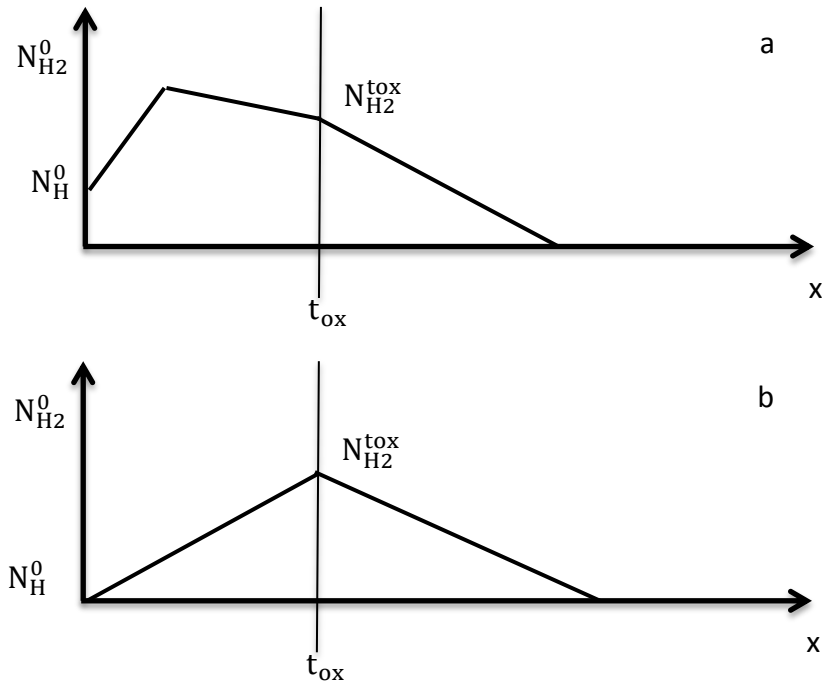

Figure V.5 Schematic representation of the Hydrogen species profile during the recovery phase.

V.5 CONCLUSION

The NBTI degradation in pure SiO_2 is proposed to be ascribed only to one mechanism which is related to the interface creation and subsequent diffusion of the released hydrogen species. The introduction for nitrogen complicates the nature of the NBTI degradation.

A proposed model is given. It is built around the classical Reaction-diffusion plate-form. It takes into consideration the non-instantaneous transformation of H to H_2 and the diffusion in the polysilicon gate. Simulation and model discussion are found in the next chapter.

CHAPTER VI

MODEL SIMULATION AND RESULTS

VI.1 INTRODUCTION

In reliability studies, numerical simulators are often used to verify the accuracy of the proposed mathematical-based models.

In this chapter the proposed model is implemented into COMSOL Multiphysics simulator. Results obtained are compared with classical R-D model and discussion of the model is given.

VI.2 COMSOL MULTIPHYSICS SIMULATOR

COMSOL Multiphysics is a powerful interactive environment for modeling and solving all kinds of problem based on partial differential equations (PDEs). The underlying mathematical structure in COMSOL Multiphysics is described through the following PDE modes:

- Coefficient form.
- General form.
- Weak form, for models with PDEs on boundaries, edges, or points

To solve the PDEs, COMSOL Multiphysics uses the finite element method (FEM). The software runs the finite element analysis together with adaptive meshing and error control using a variety of numerical solvers.

The basic flow of actions to be followed to accomplish model simulation is summarized below:

- **Model Navigator:** It is the starting point for a new model. At this step one is able to select application modes and specify variable names and other model properties in the Model Navigator.
- **Options and Settings:** Here the basic settings are defined, for example, the axis or grid spacing settings, constants and variables. These can usually be made with commands from the Options menu.
- **Geometry Modeling:** Here one creates the model geometry using the CAD tools on the draw menu and the draw toolbar**.**
- **Physics Modeling:** In this step one enters all the descriptions and settings for the physics and equations in the model. This part contains one or more of the following sections:
    - **Subdomain Settings:** In this section one specifies subdomain settings. They describe material properties, sources, and PDE coefficients on the subdomains. On the subdomains it is also possible to specify initial condition and element types.
    - **Boundary Conditions:** Here one specifies boundary and interface conditions.
- **Mesh Generation:** Here one creates the finite element mesh for the model geometry.
- **Computing the Solution:** Here one could choose between various solvers in COMSOL Multiphysics to compile and solve the model.
- **Postprocessing and Visualization**: Here one makes the visualization settings as well as performs various postprocessing of the analysis results. One works with the Plot Parameters dialog box and other visualization and postprocessing tools**.**

VI.3 CLASSICAL R-D MODEL SIMULATION

Before simulating the proposed model, it is essential to first simulate the classical R-D model to clarify the weakness that it is suffers.

Figure VI.1 illustrates the system of differential equations to be implemented in COMSOL to simulate the classical R-D

The report generated by the COMSOL software for the classical model is given in appendix 1. I used the version 3.1 of the COMSOL.

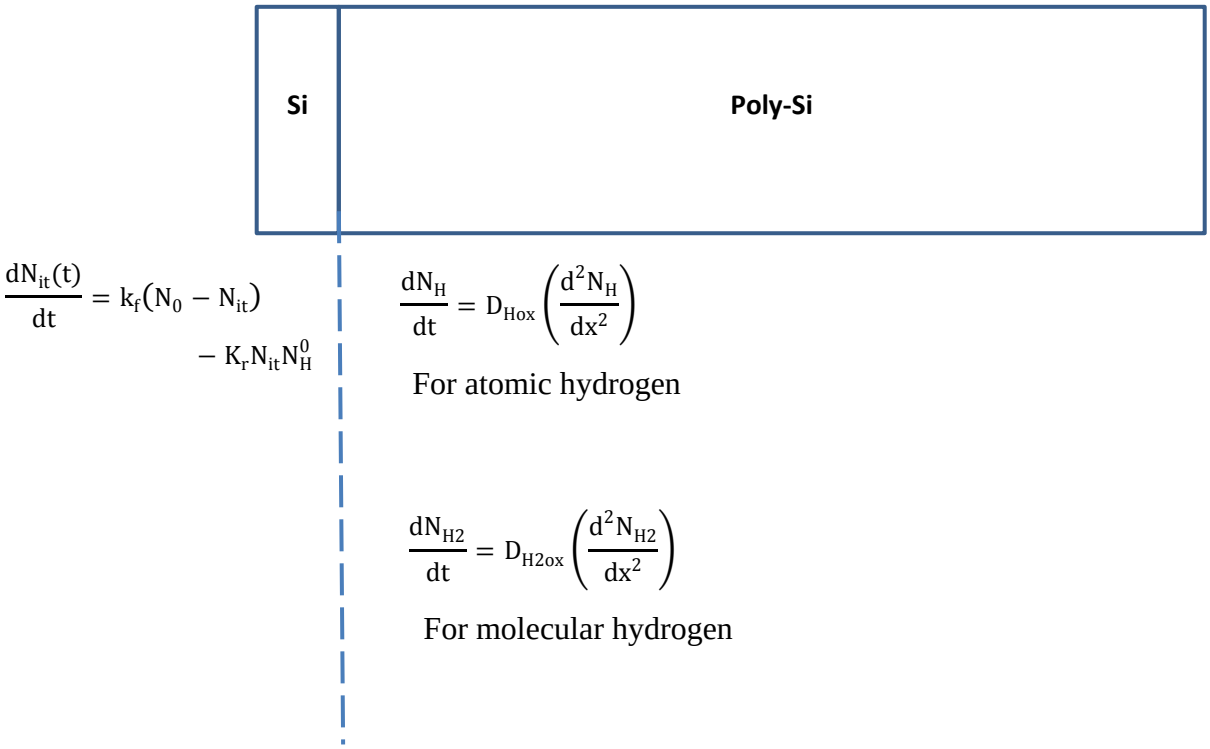

Figure VI.1 Schematic representation of the physics of the classical model for pure SiO_2 at the interface and in the oxide bulk

To implement the classical R-D, we follow the flow of actions defined in the previous section with the following parameters:

- Dependent variables:
  - N_{it}: Interface traps concentration at the interface.

- N_H: Atomic hydrogen concentration in the oxide bulk.
- N_{H2}: Molecular hydrogen concentration in the oxide.

- Physics of the model
  - Diffusion for N_H and N_{H2}
  - Weak Form boundary defined at the Si-SiO_2 interface for N_{it}.

    The weak form, which is a powerful feature of COMSOL, is used to simulate the interface trap generation at the interface (boundary 1).

- Constants:

  $k_f = 10^{-1}s^{-1}$:Forward rate reaction.

  $k_r = 8\ 10^{-3}cm^3.s^{-1}$:Backward reaction rate.

  $D_H = 2.8\ 10^{-14}\ cm^2.s^{-1}$: Atomic hydrogen diffusivity.

  $D_{H2} = 4\ 10^{-14}\ cm^2.s^{-1}$: Molecular hydrogen diffusivity.

  $N_0 = 10^{14}\ cm^{-2}$:Initial available Si-H bonds density.

- Variables:

  To simulate the rate of interface generation, a boundary variable "Reaction" at boundary number '1' is defined as:

  $$Reaction = K_f(N_0\text{-}Nit)\text{-}K_r\ N_{it}\ N_H$$

- **Geometry :**

  The geometry is 2D problem. The first edge (boundary 1) represents the Si-SiO_2 interface

- **Postprocessing and Visualization**

The simulation of the reaction regime is shown in Figure VI.2.

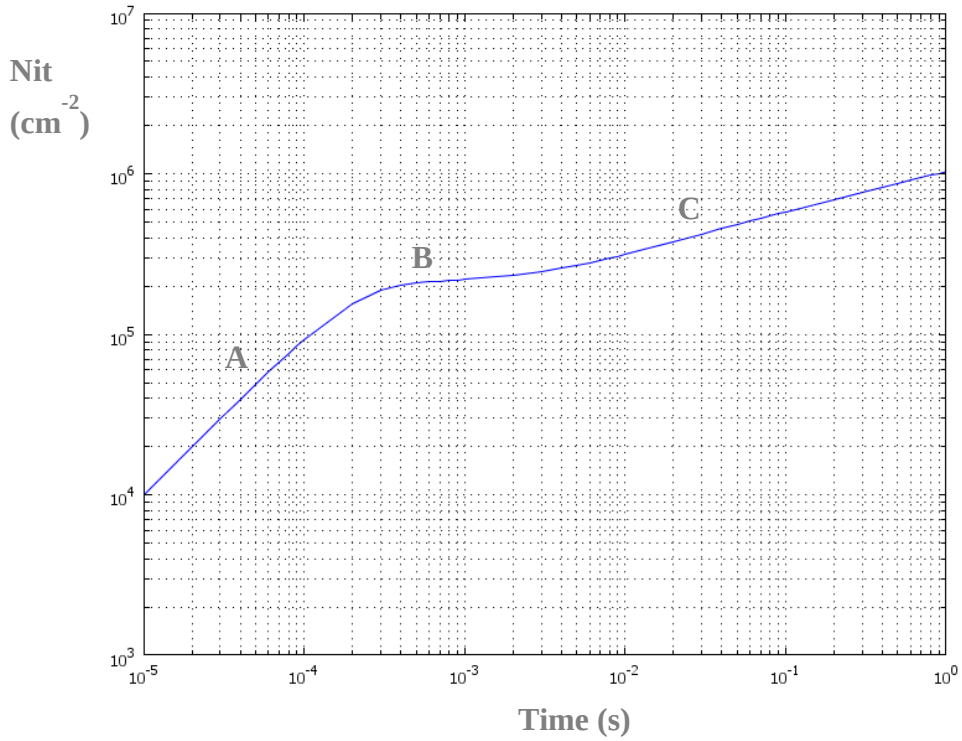

Figure VI.2 Simulation of the classical R-D model at the reaction regime

Just after the application of the stress, atomic hydrogen H^0 is created at the interface according to equation (V.2), the degradation is reaction limited. (Regime A in figure VI.2). These atoms continue to pile up at the interface until the forward and backward rates are equal, afterward the H^0 concentration remains constant during this time, which is very short (Regime B in figure VI.2).

Depending on their diffusivity coefficient, the hydrogen atoms start to move away from the interface causing the hydrogen concentration at the interface to be decreased. As a result, the backward rate in equation (V.2) becomes smaller; hence more hydrogen atoms should be produced to obtain back the quasi-equilibrium. The more the hydrogen species diffuse away the more interface traps are generated. The degradation is limited by the diffusion of the hydrogen. (Regime C in figure VI.2).

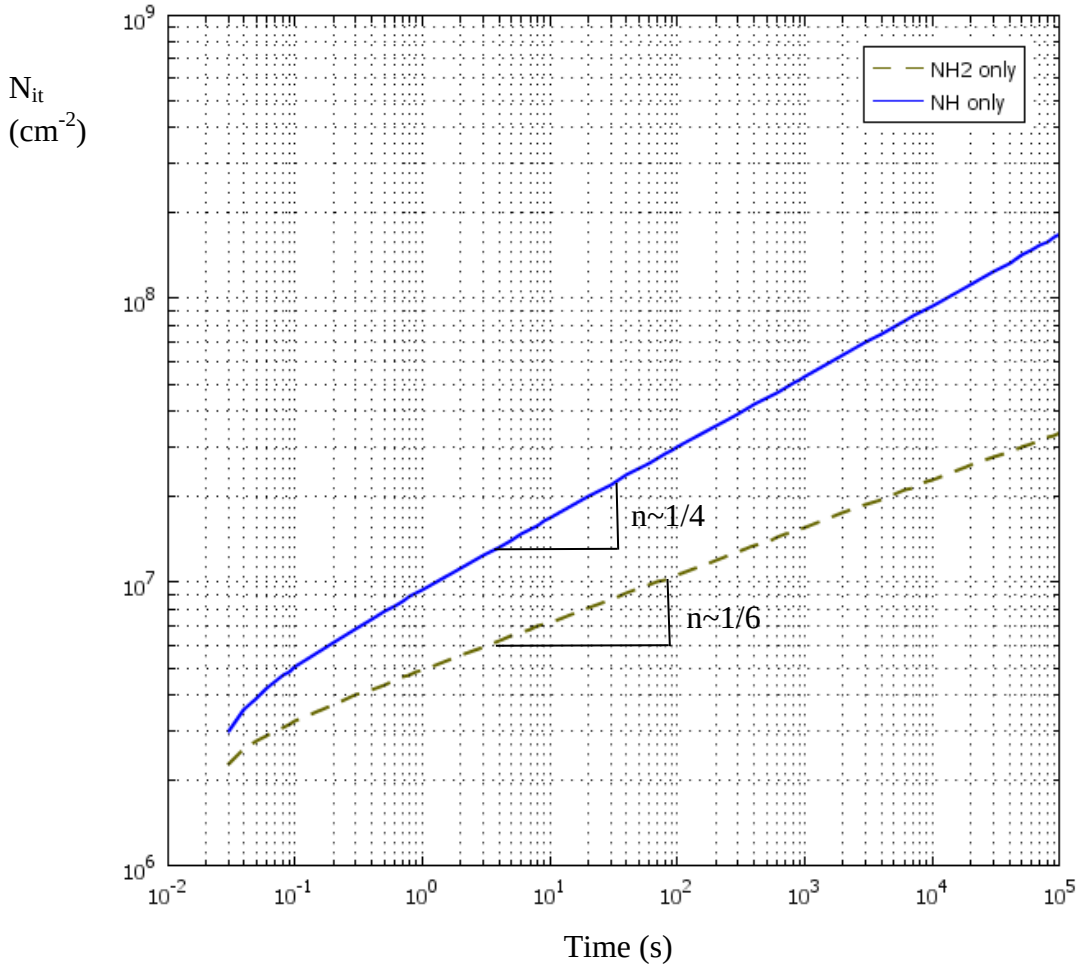

Figure VI.3 Simulation result of the classical R-D model at the diffusion phase

For longer stress time, Figure VI.3 shows the simulation results of the R-D model highlighting the different behavior of degradation when atomic hydrogen or molecular hydrogen diffusion species are used. As predicted by the classical Reaction-Diffusion model, the time exponent is about 1/4 when the diffusion species are atomic hydrogen H (H only) and 1/6 when they are molecular hydrogen (H_2 only).

Figure VI.3 shows one of the weaknesses of the classical R-D. It fails to reproduce the Initial higher slope (within 10 s).The proposed model overcome this point.

Figure VI.4 depicts the hydrogen profile after 0, 10, 100 and 1000 seconds of stress. Again this figure demonstrates the validity of the hydrogen triangular profile approximation used to derive the analytical expression of the NBTI degradation.

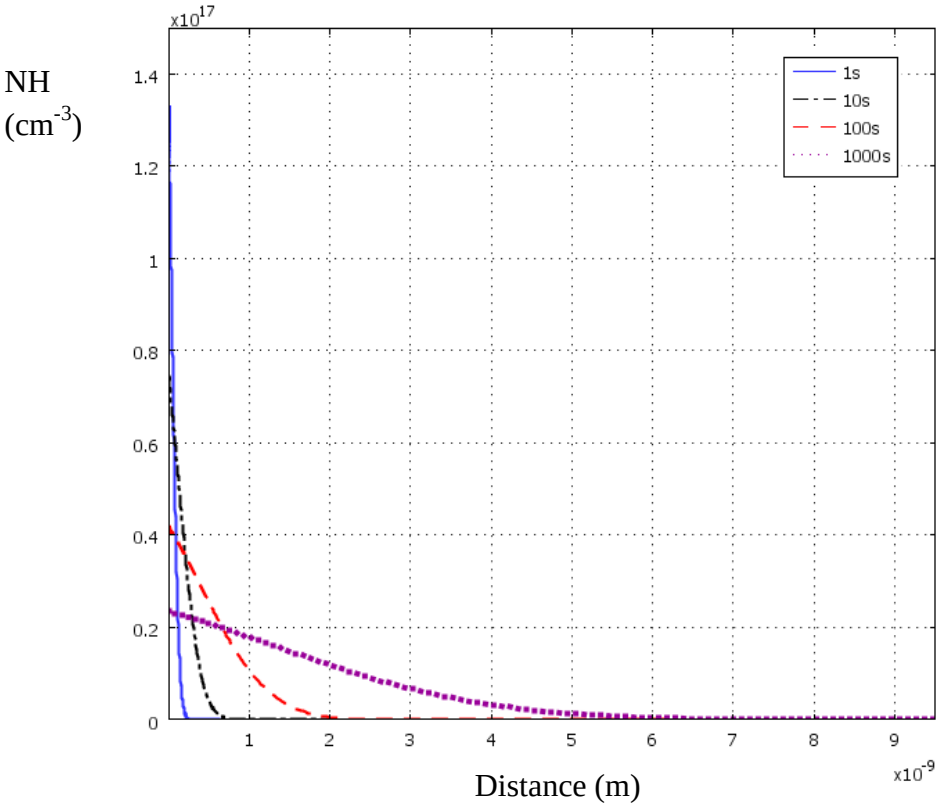

Figure VI.4 Hydrogen profile after different time of stress.

Finally, Figure VI.5 is a simulation result of the recovery of NBTI in the context of classical R-D. The stress is turned off after 1000 s for another 1000 s.

The recovery phase is one of weakest point for classical R-D model. In contrast to experimental result no fast recovery regime is observed, as well as, after the same period of stress only about 50% of the stress-induced interface trap are recovered. These weaknesses are resolved in the context of the proposed model.

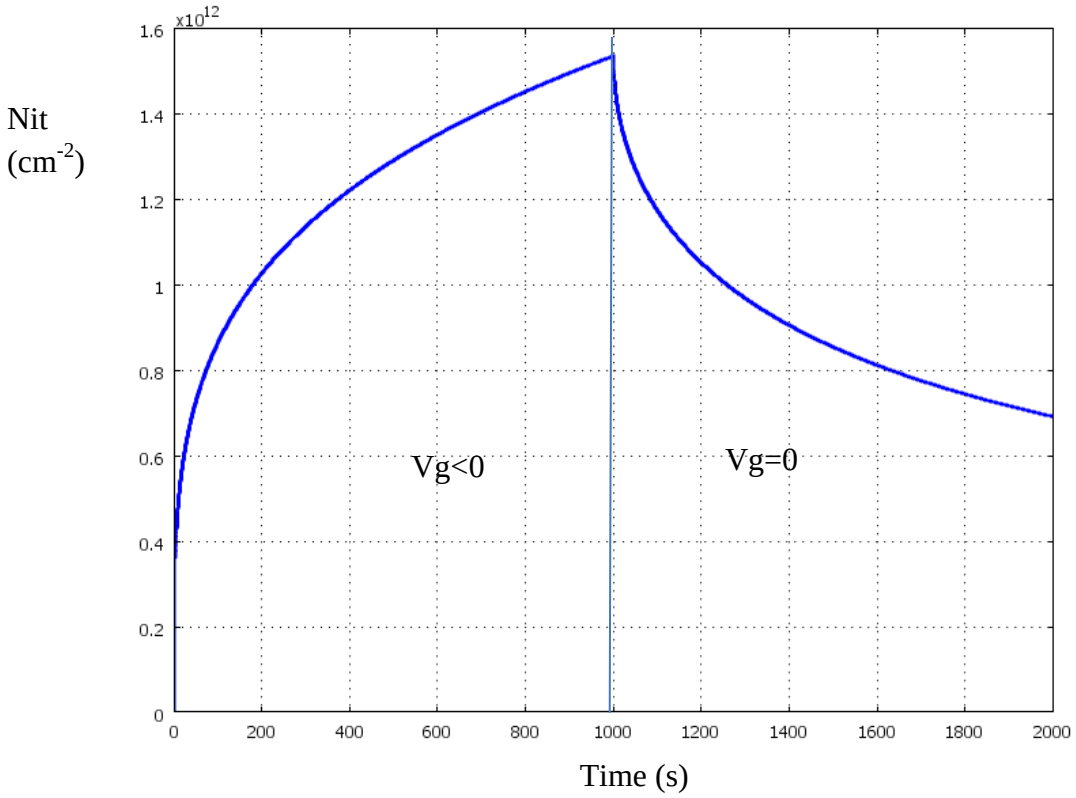

Figure VI.5 Simulation of the recovery behavior of the NBTI in the context of the R-D model

Figure VI.6 sketches the hydrogen profile after 0, 1, 10, 100 and 1000 seconds of recovery. This figure shows clearly that although the hydrogen diffuses back to the interface, the front end continues to diffuse away.

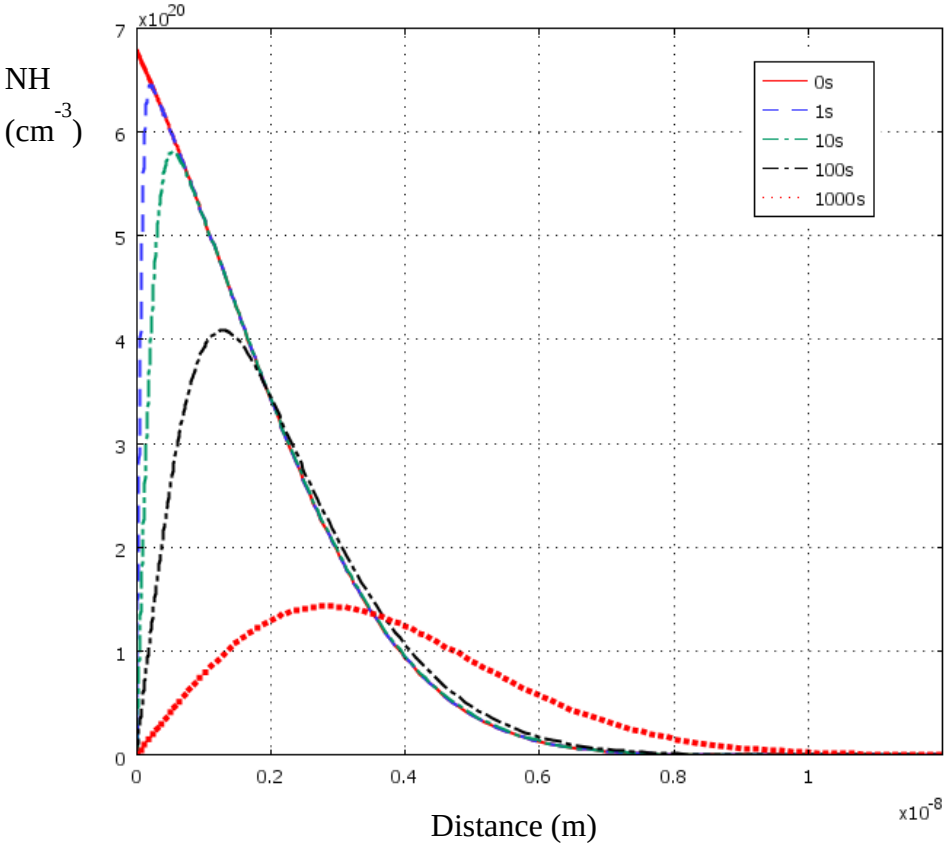

Figure VI.6 Hydrogen profile after 0, 1, 10, 100 and 1000 seconds of recovery.

VI.4 MODIFIED R-D MODEL SIMULATION

The proposed model equations that are executed by the COMSOL Multiphysics are summarized in the figure VI.7

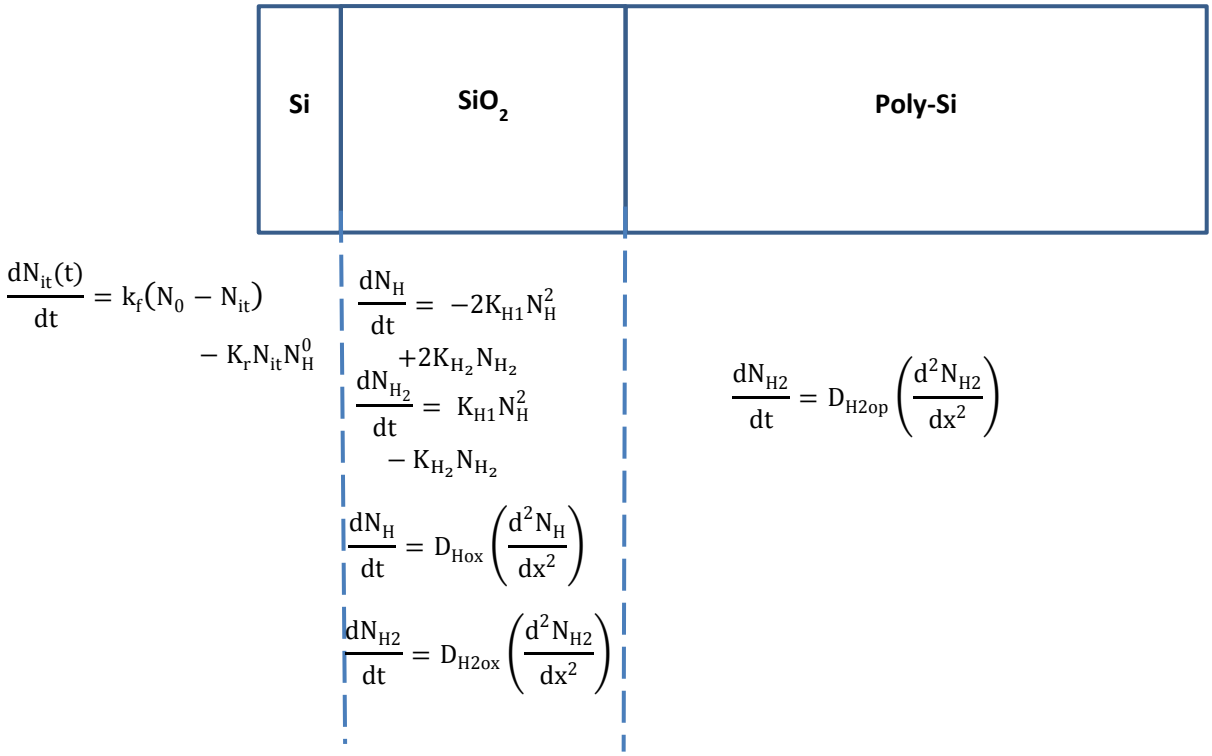

Figure VI.7 Schematic representation of the physics of the proposed model for pure SiO_2 at the interface, in the oxide bulk and in the polysilicon gate.

To implement the proposed model, I have followed the same flow of actions defined in the previous section with the following parameters:

- Dependent variables:
  - N_{it}: Interface traps concentration at the interface.
  - N_H: Atomic hydrogen concentration in the oxide bulk.
  - N_{H2}: Molecular hydrogen concentration in the oxide and the polysilicon.
- Physics of the model
  - Diffusion for N_H and N_{H2}
  - Weak Form boundary defined at the Si-SiO_2 interface for Nit.
- Constants:

  $K_f = 10^{-1} s^{-1}$:Forward rate reaction.

  $K_r = 8\ 10^{-3} cm^3.s^{-1}$:Backward reaction rate.

  $D_H = 2.8\ 10^{-14}\ cm^2.s^{-1}$: Atomic hydrogen diffusivity.

  $D_{H2} = 4\ 10^{-14}\ cm^2.s^{-1}$: Molecular hydrogen diffusivity.

$K_{H1}= 10^{-5}cm^3.s^{-1}$: the rate of H to H_2 transformation.

$K_{H2}= 10^{-1}\ s^{-1}$.: the rate of H_2 to H transformation.

$N_0 = 10^{14}\ cm^{-2}$:Initial available Si-H bonds density.

- Variables:

To simulate the rate of interface generation, a boundary variable "Reaction" at boundary number '1' is defined as:

$$Reaction = k_f(N_0\text{-}Nit)\text{-}k_r\ N_{it}\ N_H$$

- **Geometry :**

The geometry is simple line (1D problem) in the x-direction. It consists of two adjacent subdomains (lines) one of 1.3 nm of length to represent the oxide and the other of 10 nm to represent the polysilicon. Figure VI.8

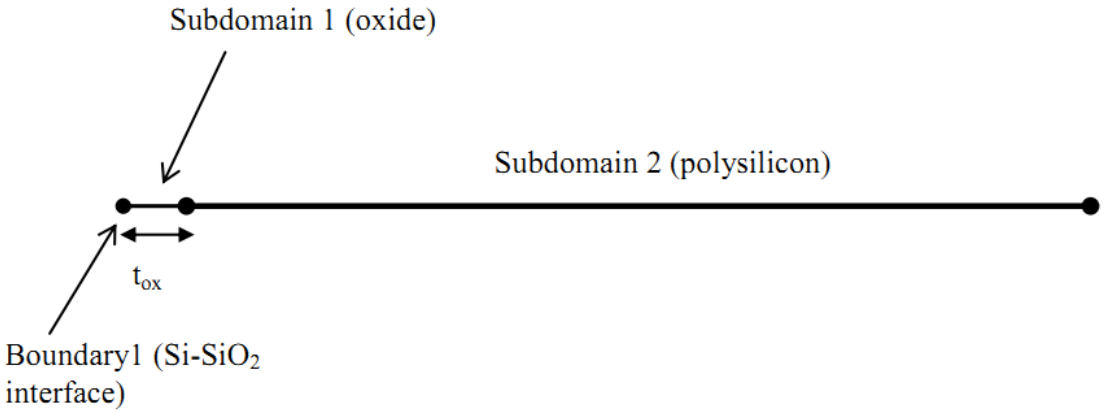

Figure VI.8 Geometry definition of the proposed model used in Comsol simulation.

- **Postprocessing and Visualization**

The reaction phase of the proposed model is the same as the reaction phase of the classical R-D model.

For the diffusion phase, the released H atoms, while diffusing away from the interface, can get converted into H_2, because neutral H atom is thought to be unstable [41] taking into consideration that that H_2 cannot be formed directly from the Si–H breaking nor it can passivate an interface trap. In turn, the molecular H_2 can also diffuses or dissociates back to H atoms. From chapter IV, we know the H-only and H_2-only diffusion models give the time-exponents of 1/4 and 1/6, respectively. For the proposed model, the H-only and H_2-only curves act as limits to the model. That is, when k_{H1} in equation V.4 reduces toward

zero the solution approaches that of H-only. Similarly, when k_{H1} is increased further so that more H is consumed the degradation approaches to the H_2-only result. This stage of degradation lasts as long as the front end of the diffusion species does not reach the oxide-polysilicon interface (figure VI.9).

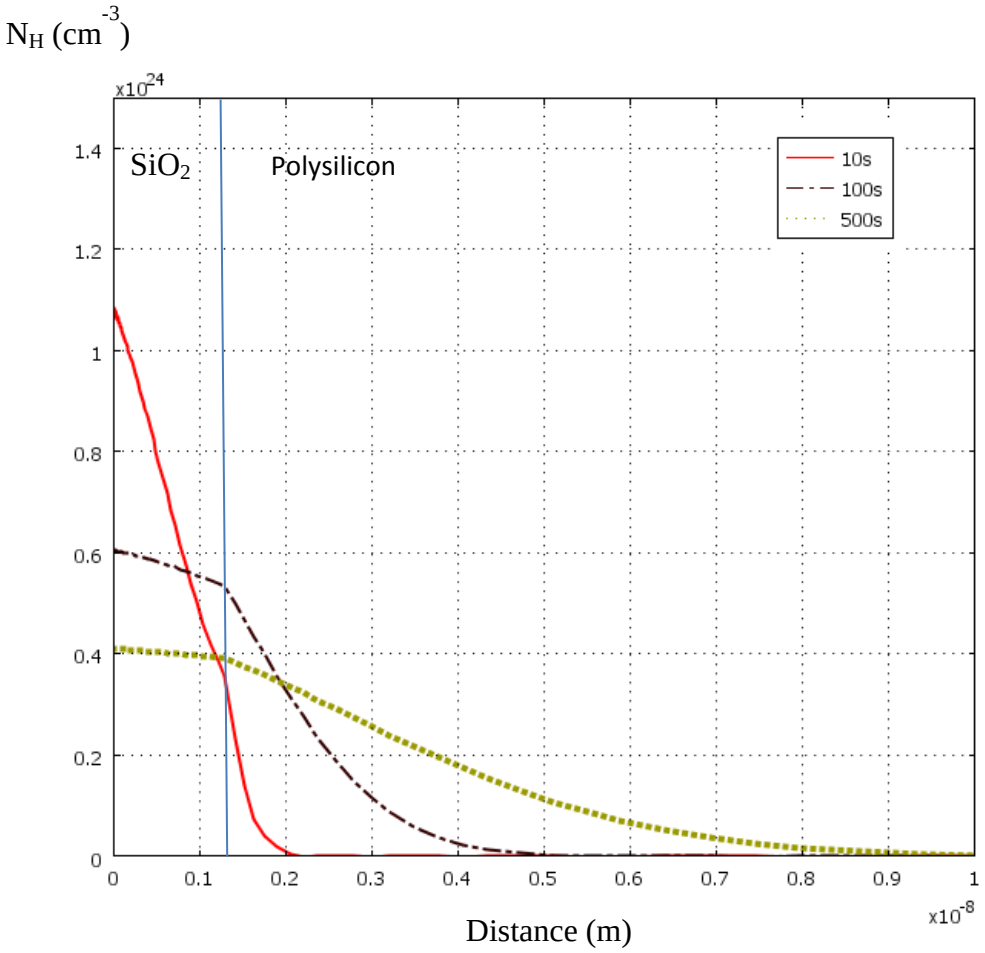

Figure VI.9 Hydrogen profile after different time of stress in both oxide and polysilicon in the context of the modified model.

Once the front of the diffusion hydrogen reaches the interface, it moves into the poly-silicon gate, which is characterized by the diffusing coefficient lower than in the oxide bulk.

$$D_p < D_{H2_{ox}}$$

As a consequence of the difference between the diffusing coefficients, H_2 molecules move slower in the ploy-silicon than they do in the oxide. Hence H_2 start to pile up in the oxide,

until it reaches the saturation level, while continuing to diffuse in the polysilicon. The simulation results of this phase are shown in figure VI.9.

Figure VI.10 represents the simulation result during 10^3 s of stress time. It is clearly shown that the slope is higher in the initial phase (t<10 s) than it is in the later phase of stress. This model succeeds in predicting the higher time-exponent at early stage of the stress (within 10 s). This regime of higher exponent is the consequence of the initial transformation of H to H_2. The subsequent regime is governed by the diffusion of H_2 in the polysilicon which is characterized by the robust time-exponent of 1/6.

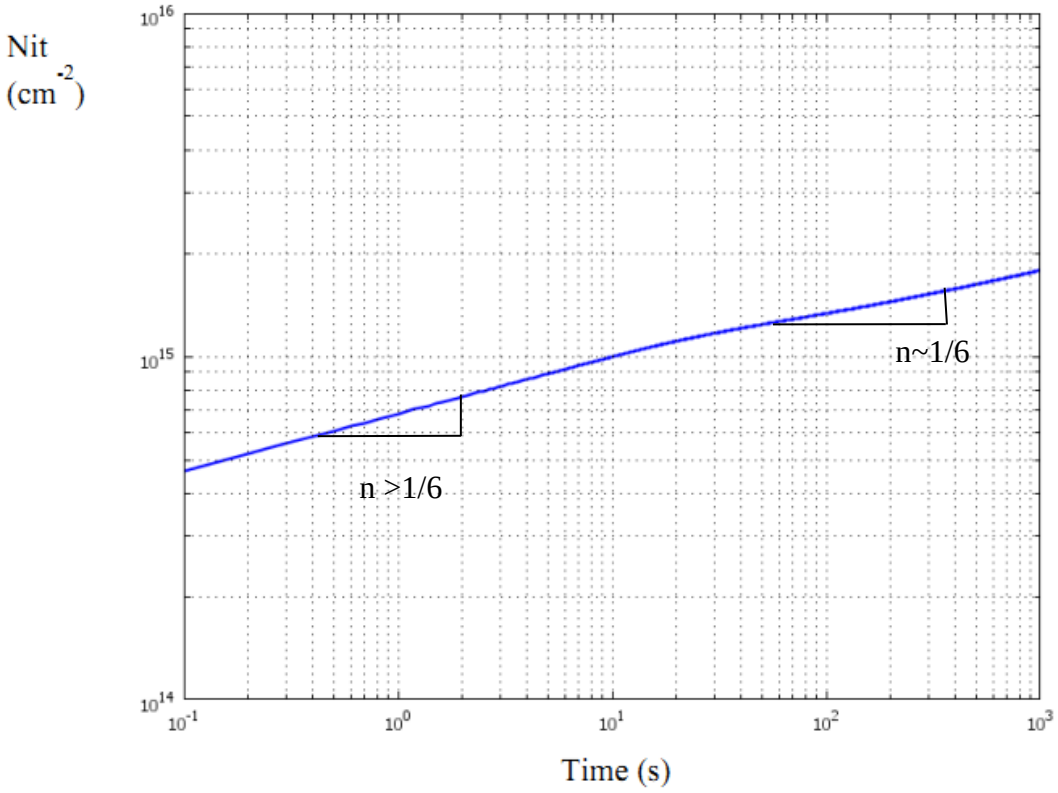

Figure VI.10 Simulation of the interface trap generation in the context of the proposed model.

For the recovery phase, the stress is turned off. No further generation of hydrogen at the Si-SiO_2 interface is taking place because the generation term in equation (V.2) is zero. Hydrogen atoms at the interface are consumed to repassivates the silicon dangling bonds. Hydrogen atoms in the oxide bulk diffuse back to the Si-SiO_2 interface. Because of the

different diffusing coefficient, at early time the hydrogen species in the oxide bulk diffuse back to the interface while the hydrogen molecules continue to diffuse away from the interface. The simulation results are presented in figure VI.11

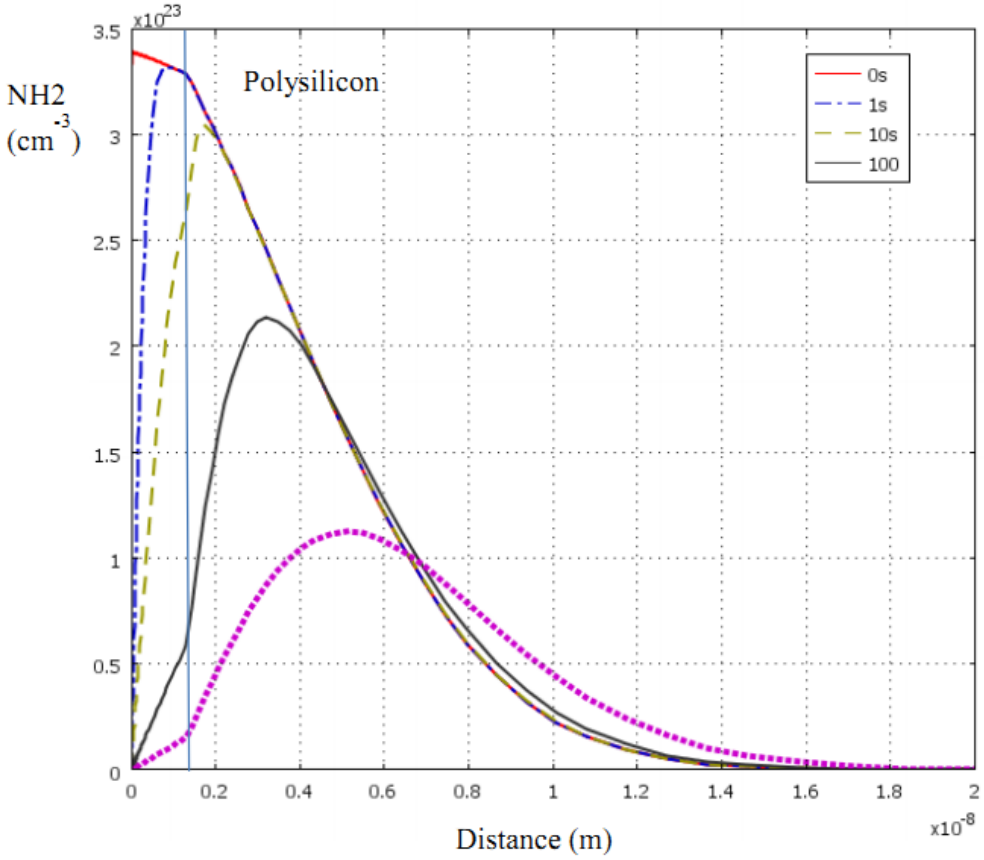

Figure VI.11 Hydrogen profile after different time of recovery in both oxides and polysilicon in the context of the modified model

Figure VI.12 is simulation of the recovery phase. It shows a rapid decay of the characteristic after stopping the stress. In addition, for the same time of relaxation as for stress, the results show more recovery (about 70%) than obtained for the classical model.

A key feature in the recovery phase that is worth noticing is the hydrogen species in the oxide diffuse back rapidly due to their higher diffusivity coefficient. The subsequent recovery is limited by the back diffusion of hydrogen molecules in the poly silicon oxide.

This explains the fast annealing of interface traps density at the early stage of the recovery. The slow recovery is governed by the diffusion in the poly silicon.

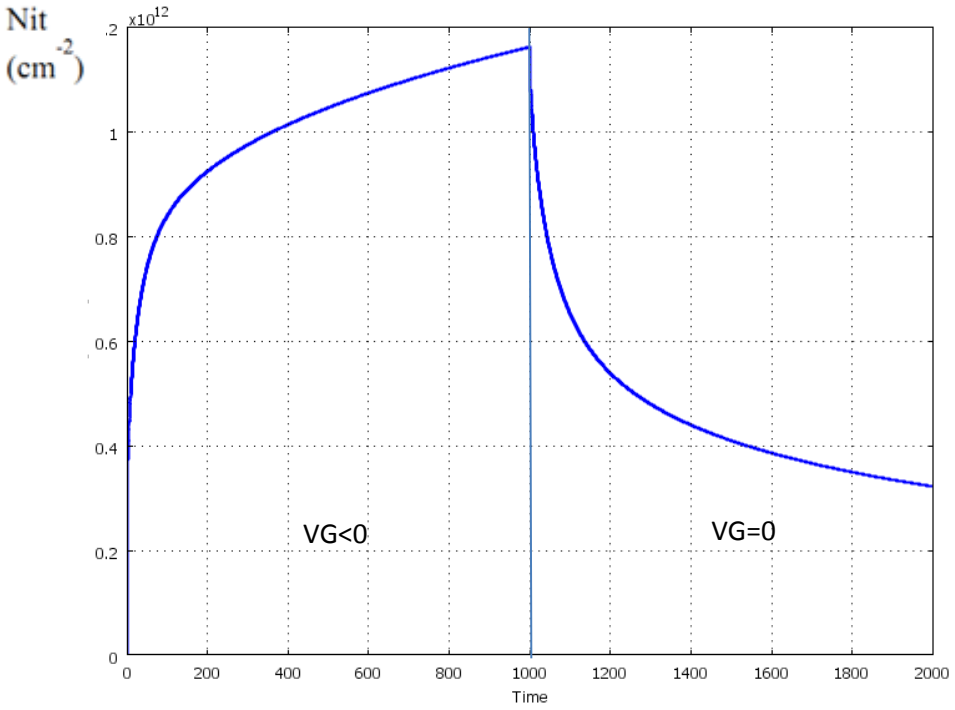

Figure VI.12 Simulation of the recovery of NBTI degradation of the proposed model,

The following table compares the proposed model with the classical R-D model:

Classical R-D model	Proposed model
Failed to predict the higher initial time exponent (<10 s). Figure VI.3	Better predicts the initial phase. Figure VI.10
Failed to predict the fast initial recovery just after turning off the stress. Figure VI.5	Faster initial recovery is predicted. Figure VI.11 and figure VI.12
After the same period of stress only about 50% of the stress-induced interface trap are recovered. Figure VI.5	After the same period of stress more than 70% of the stress-induced interface trap are recovered. Figure VI.12

Table VI.1 Comparison between the proposed model and the classical R-D model.

VI.5 CONCLUSION

Negative bias temperature instability in pure-SiO_2 is proved to be ascribed to one mechanism which is believed to be related to Si-H bonds dissociation at the interface. One prominent model is the reaction-diffusion (RD) theory which has been given much attention and refinement since first proposed.

The proposed model modifies two assumptions used in stating the classical R-D:

- Rather than Instantaneous transformation of the released atomic hydrogen to molecular ones, the proposed model takes the non-instantaneous H-H_2 transformation into consideration.
- Rather than infinite oxide thickness, the proposed model is based on the realistic finite oxide thickness and the diffusion of H_2 into polysilicon.

The simulation results clearly support the validity of the model. The proposed model improves the classical R-D toward better predicting:

- The initial higher slope for the stress period.
- The rapid decrease of interface traps concentration after removing the stress.
- The recoverable amount of interface for the same recovery period as stress period.

CHAPTER VII

CONCLUSION

The objective of this thesis concerned the evaluation of a new model for the Negative Bias Temperature in pure-oxide. The work performed during this thesis allowed us to study in depth the NBTI from the microscopic defects related to NBTI to the simulation of the proposed model.

Oxide and interface defects suspected to be behind the NBTI are studied. P_b and E' defects are electrically active defects. Their density and distribution in the oxide depends on the oxidation process especially the annealing phase.

NBTI is distinguished from other reliability problem by the fact that under moderate negative bias and relatively high temperature it shows the following characteristics:

- Power law behavior of the time evolution when plotted on a log-log scale. Different values of the time exponent have been quoted. They range from 0.25 to 0.1.
- Initial high time exponent (with in 10s).
- Logarithmic time dependence of the recovery
- Temperature activated process.

The modeling of the NBTI is a problematic task because:

- NBTI recovery makes the experimental data less accurate even when ultrafast switching or On-The-Fly methods are used.
- NBTI hardly dependent on the oxidation process. Pb, E' and nitrogen concentration and their distribution in the oxide is proved to influence NBTI degradation.

Reaction-Diffusion model is wildly accepted to better reproduce the NBTI behavior. It is based on the dissociation of Si-H bonds to P_b centers and free hydrogen atoms and the subsequent diffusion of the H into the oxide. Nevertheless many attempts are done to rise up the role of E' centers in the degradation. E' center under this context plays the role of switching trap for the trapping detrapping of a hole process.

None of the available models succeed in explaining all of the experimental observation. I focused on the NBTI in pure-SiO_2 and demonstrated that NBTI:

- caused only by one mechanism,
- related to P_b center creation, and
- limited by neutral species diffusion

I proposed a model that is built on the classical Reaction-diffusion plate-form. The NBTI degradation in pure -SiO_2 is demonstrated to be ascribed only to one mechanism which is related to the interface creation and subsequent diffusion of the released hydrogen species.

The proposed model takes into consideration the non-instantaneous transformation of H to H_2 and the diffusion in the polysilicon gate.

The simulation results obtained using COMSOL Multiphysics clearly highlights the benefits of the proposed model. It improves the classical R-D toward better predicting:

- The initial higher slope for the stress period.
- The rapid decrease of interface traps concentration after removing the stress.
- The recoverable amount of interface for the same recovery period as stress period.

In spite of the improvements added by the proposed model to the classical R-D, it still suffers from some weaknesses especially during the recovery stress. It is worth noticing that the proposed model is useful only for pure-SiO_2. However, the oxides, used in modern devices, are usually doped with impurities, especially with nitrogen, to allow further scaling down. Therefore the study of the effects of such impurities on the NBTI should be included to the proposed model. This can be done by comparing the NBTI behavior of pure and doped oxides of the same thickness, under the same stress conditions and using the same technique of characterization.

In general, the nitrogen addition could affect the original mechanism in pure SiO_2 by:

- Enhancing it.
- Suppressing it and creation of a new one.
- Not affecting it and adding new one.

To verify which of these scenarios would occur, experiments should be performed.

Based on theoretical reasoning and on the proposed model, I would suggest that:

- The nitrogen introduction cannot enhance the degradation caused by the original mechanism because of two reasons: The first one is that most of the diffusion of the hydrogen occurs in the polysilicon which is nitrogen free. The second one is that the NBTI is limited by the diffusion of hydrogen molecules in the polysilicon oxide.
- In the case when the nitrogen introduction suppresses the original mechanism and adds a new one, then, there will be no difference between NBTI degradation in thick and thin oxides.
- If the nitrogen introduction adds a new mechanism to the original one, then the nitrogen contribution to the NBTI degradation could be extracted out by comparing two devices of thick and thin oxides.

Appendix 1

COMSOL GENERATED REPORT OF THE CLASSICAL R-D

Classical R-D

1. Table of Contents

2. Model Properties

Property	**Value**
Model name	Classical R-D
Author	M.MELLATI
Company	
Department	
Reference	
URL	
Saved date	Dec 17, 2011 4:44:31 PM
Creation date	Dec 17, 2011 3:04:49 PM
COMSOL version	COMSOL 3.3.0.405

Application modes and modules used in this model:

- Geom1 (2D)
  - Diffusion
  - Weak Form, Boundary

3. Constants

Name	Expression	Value	Description
Kr	8e-3[cm^3/s]	8e-9[m^3/s]	Backward reaction rate
DH2	4e-14[cm^2/s]	4e-18[m^2/s]	H2 diffusivity
DH	2.8e-14[cm^2/s]	2.8e-18[m^2/s]	H diffusivity
N0	1e14[cm^-2]	10e17[1/m^2]	Initial intrerface trap density

4. Global Expressions

Name	Expression	Description
Kf	(1e-1*(t<=1000)+0*(t>1000))[1/s]	

5. Geometry

Number of geometries: 1

5.1. Geom1

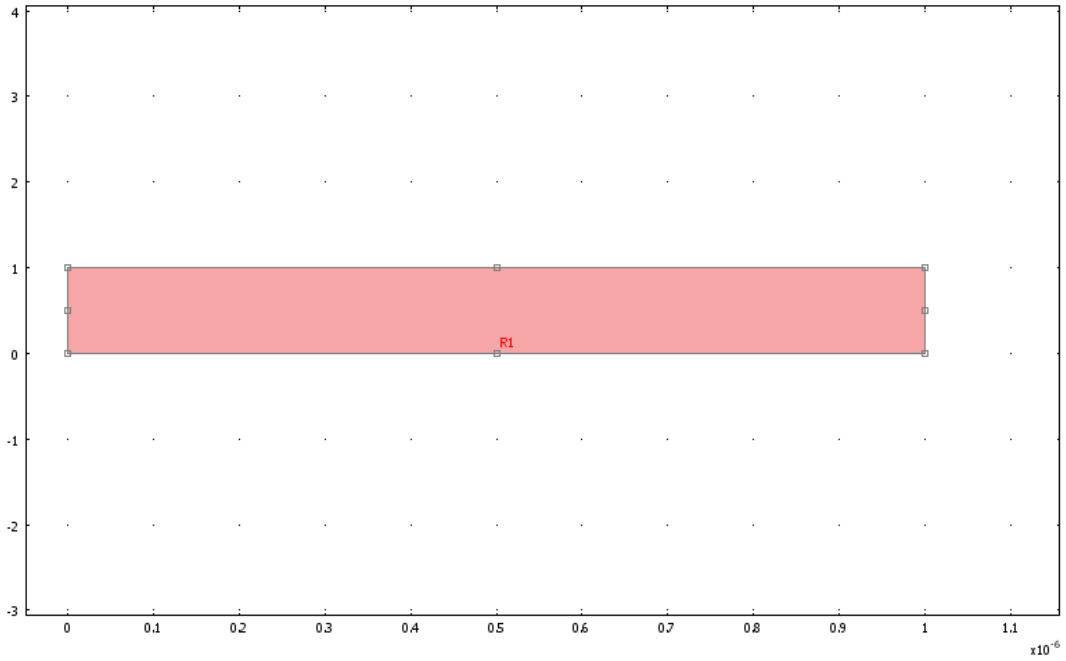

5.1.3. Subdomain mode

6. Geom1

Space dimensions: 2D

Independent variables: x, y, z

6.1. Expressions

6.1.1. Boundary Expressions

Boundary	1
Reaction	Kf*(N0-Nit)-Kr*Nit*NH

6.2. Mesh

6.2.1. Mesh Statistics

Number of degrees of freedom	416
Number of mesh points	112
Number of elements	172

Triangular	172
Quadrilateral	0
Number of boundary elements	50
Number of vertex elements	4
Minimum element quality	0.754
Element area ratio	0.012

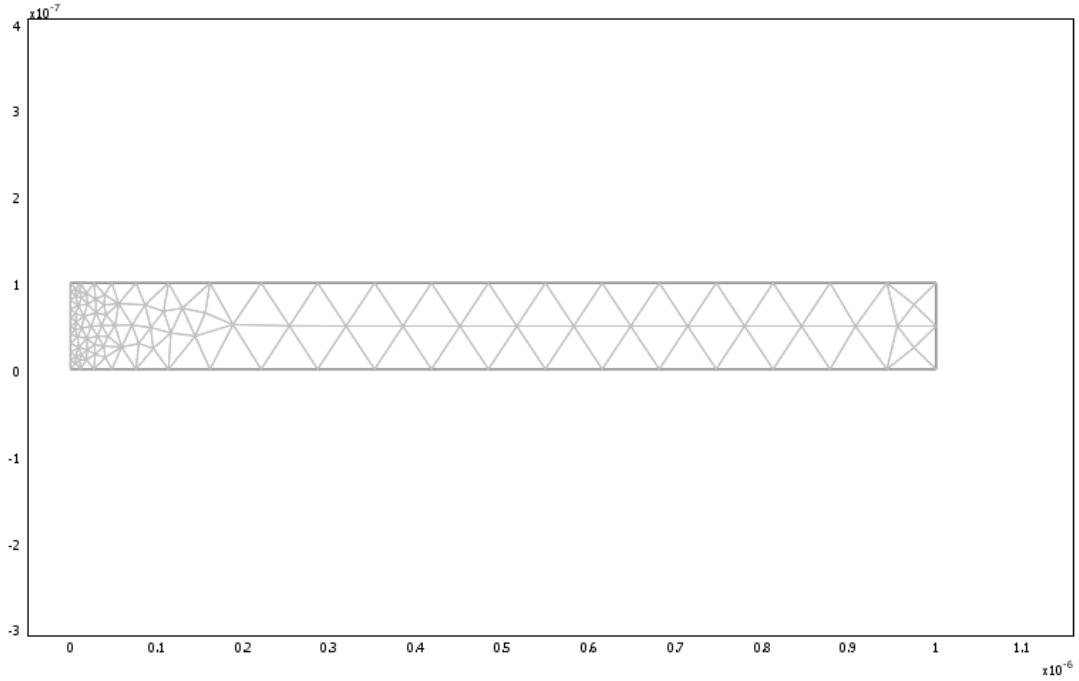

6.3. Application Mode: Diffusion (di)

Application mode type: Diffusion

Application mode name: di

6.3.1. Application Mode Properties

Property	**Value**
Default element type	Lagrange - Quadratic
Analysis type	Transient

Frame	Frame (ref)
Weak constraints	Off

6.3.2. Variables

Dependent variables: NH

Shape functions: shlag(2,'NH')

Interior boundaries not active

6.3.3. Boundary Settings

Boundary		2-4	1
Type		Insulation/Symmetry	Flux
Inward flux (N)	$mol/(m^2 \cdot s)$	0	**Reaction**

6.3.4. Subdomain Settings

Subdomain		1
Diffusion coefficient (D)	m^2/s	**DH**

6.4. Application Mode: Weak Form, Boundary (wb)

Application mode type: Weak Form, Boundary

Application mode name: wb

6.4.1. Application Mode Properties

Property	**Value**
Default element type	Lagrange - Quadratic
Wave extension	Off
Frame	Frame (ref)
Weak constraints	Off

6.4.2. Variables

Dependent variables: Nit, Nit_t

Shape functions: shlag(2,'Nit')

Interior boundaries not active

6.4.3. Boundary Settings

Boundary	1
weak term (weak)	**Nit_test*Reaction**
dweak term (dweak)	**Nit_test*Nit_time**

7. Solver Settings

Solve using a script: off

Analysis type	Transient
Auto select solver	On
Solver	Time dependent
Solution form	Automatic
Symmetric	auto
Adaption	Off

7.1. Direct (UMFPACK)

Solver type: Linear system solver

Parameter	**Value**
Pivot threshold	0.1
Memory allocation factor	0.7

7.2. Time Stepping

Parameter	**Value**
Times	0:0.1:2000
Relative tolerance	0.01
Absolute tolerance	0.0010
Times to store in output	Specified times
Time steps taken by solver	Free

Manual tuning of step size	Off
Initial time step	0.0010
Maximum time step	1.0
Maximum BDF order	5
Singular mass matrix	Maybe
Consistent initialization of DAE systems	Backward Euler
Error estimation strategy	Include algebraic
Allow complex numbers	Off

7.3. Advanced

Parameter	**Value**
Constraint handling method	Elimination
Null-space function	Automatic
Assembly block size	5000
Use Hermitian transpose of constraint matrix and in symmetry detection	Off
Use complex functions with real input	Off
Stop if error due to undefined operation	On
Type of scaling	Automatic
Manual scaling	
Row equilibration	On
Manual control of reassembly	Off
Load constant	On
Constraint constant	On
Mass constant	On
Damping (mass) constant	On

Jacobian constant	On
Constraint Jacobian constant	On

8. Postprocessing

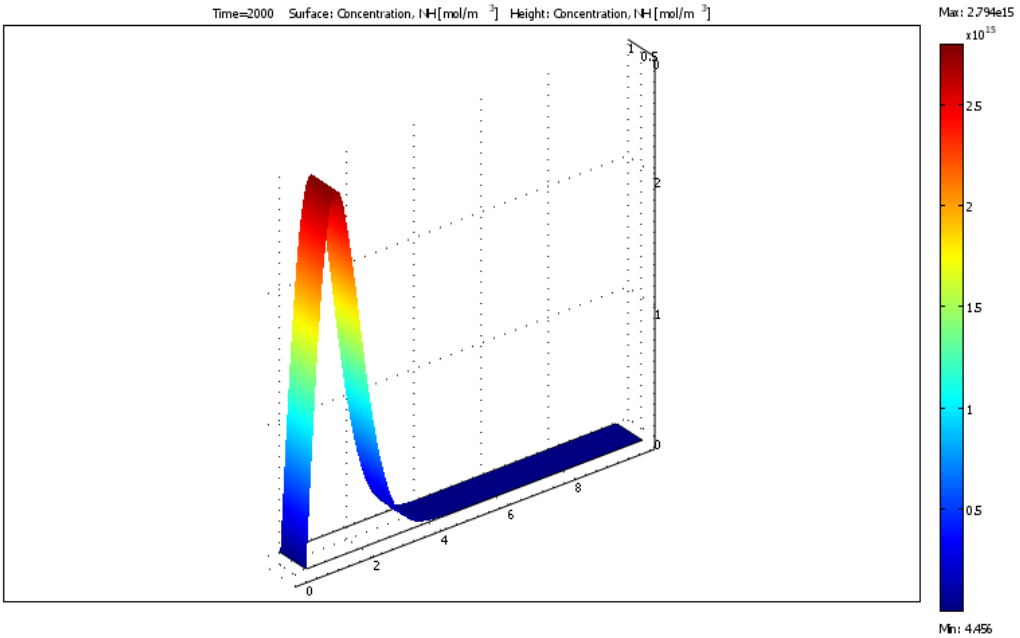

9. Variables

9.1. Boundary

Name	Description	Expression
ndflux_NH_di	Normal diffusive flux, NH	nx_di * dflux_NH_x_di+ny_di * dflux_NH_y_di

9.2. Subdomain

Name	Description	Expression
grad_NH_x_di	Concentration gradient, NH, x component	NHx
dflux_NH_x_di	Diffusive flux, NH, x component	-Dxx_NH_di * NHx-Dxy_NH_di * NHy

grad_NH_y_di	Concentration gradient, NH, y component	NHy
dflux_NH_y_di	Diffusive flux, NH, y component	-Dyx_NH_di * NHx-Dyy_NH_di * NHy
grad_NH_di	Concentration gradient, NH	sqrt(grad_NH_x_di^2+grad_NH_y_di^2)
dflux_NH_di	Diffusive flux, NH	sqrt(dflux_NH_x_di^2+dflux_NH_y_di^2)

Appendix 2

COMSOL GENERATED REPORT OF THE PROPOSED MODEL

Proposed Model

1. Table of Contents

2. Model Properties

Property	**Value**
Model name	Proposed Model
Author	MELLATI
Company	
Department	
Reference	
URL	
Saved date	Dec 31, 2011 3:46:46 PM
Creation date	Sep 4, 2011 10:47:05 AM
COMSOL version	COMSOL 3.3.0.405

Application modes and modules used in this model:

- Geom1 (1D)
  - Diffusion
  - Diffusion
  - Weak Form, Boundary

3. Constants

Name	Expression	Value	Description
Kr	8e-3 [cm^3/s]		Backward reaction rate
DH2	4e-14[cm^2/s]		H2 diffusivity in oxide
DH	2.8e-14[cm^2/s]		H diffusivity
DH2poly	1e-14[cm^2/s]		H2 diffusivity in poly
KH1	1e-5[cm^3/s]		H to H2 rate
KH2	1e-1[1/s]		H2 to H rate
N0	1e14[cm^-2]		Initial intrerface trap density

4. Geometry

Number of geometries: 1

4.1. Geom1

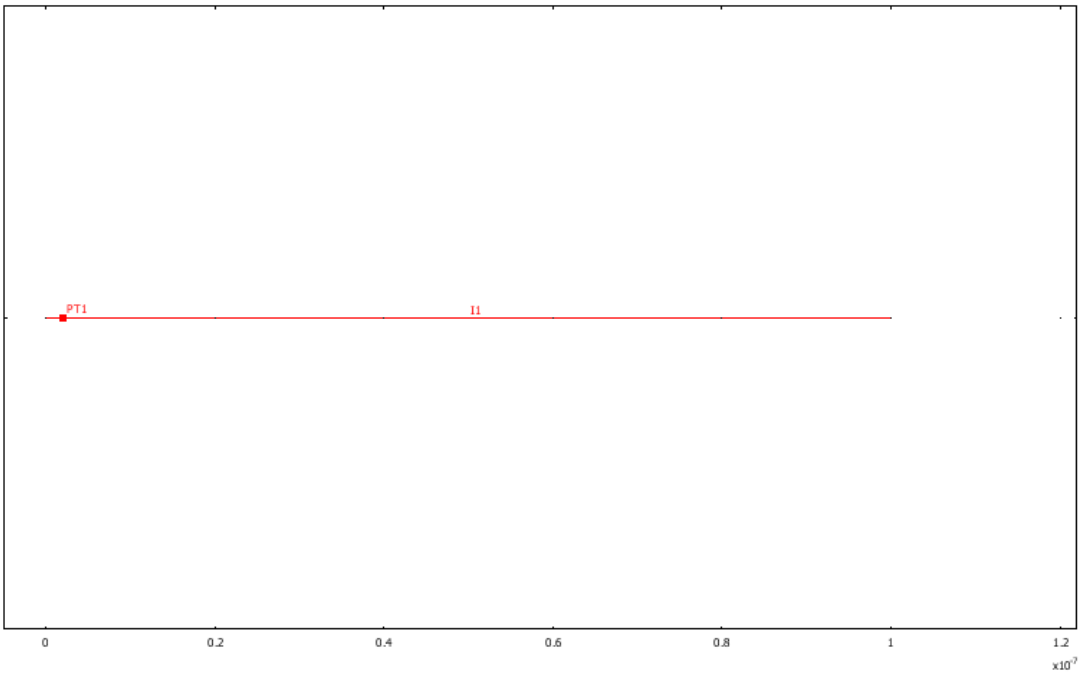

5. Geom1

Space dimensions: 1D

Independent variables: x, y, z

5.1. Expressions

5.1.1. Boundary Expressions

Boundary	1
Reaction1	Kf*(N0-Nit)-Kr*Nit*NH
Kf	1e-1*(t<=1000)

5.2. Mesh

5.2.1. Mesh Statistics

Number of degrees of freedom	3857
Number of mesh points	2105

Number of elements	2104
Number of boundary elements	3
Element length ratio	0

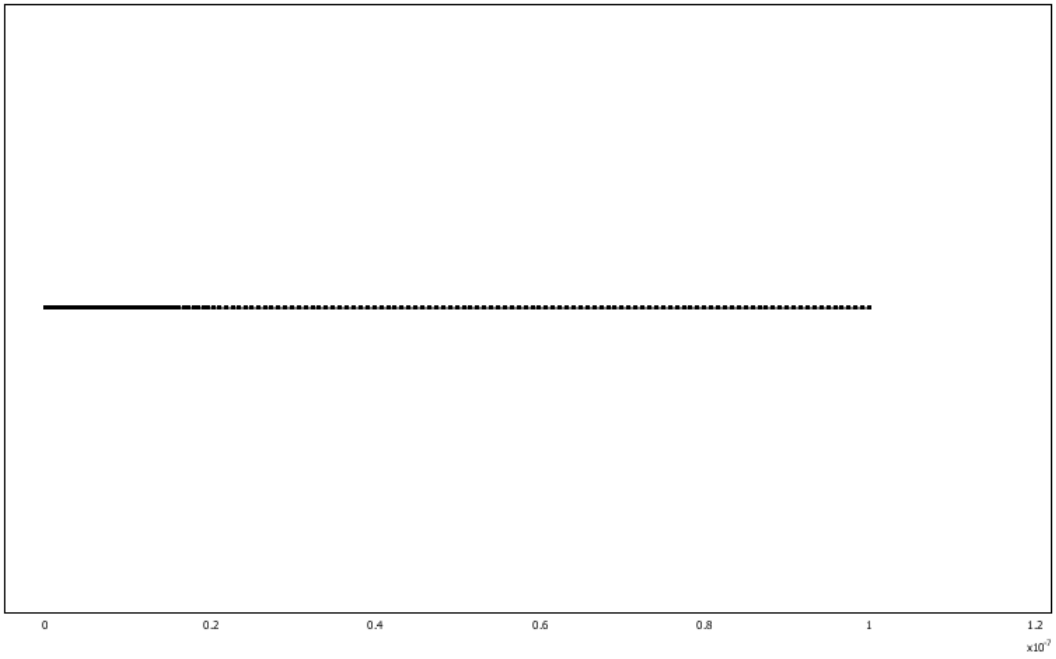

5.3. Application Mode: Diffusion (di)

Application mode type: Diffusion

Application mode name: di

5.3.1. Application Mode Properties

Property	**Value**
Default element type	Lagrange - Quadratic
Analysis type	Transient
Frame	Frame (ref)
Weak constraints	Off

5.3.2. Variables

Dependent variables: NH

Shape functions: shlag(2,'NH')

Interior boundaries not active

5.3.3. Boundary Settings

Point		1	2
Inward flux (N)	mol/(m^2·s)	**'Reaction'**	0

Point	3
Inward flux (N)	0

5.3.4. Subdomain Settings

Subdomain		1
Shape functions (shape)		**shlag(2,'NH')**
Integration order (gporder)		**4**
Constraint order (cporder)		**2**
Diffusion coefficient (D)	m^2/s	**DH**
Reaction rate (R)	mol/(m^3·s)	**2*(-KH1*NH^2+KH2*NH2)**

Subdomain initial value		1
Concentration, NH (NH)	mol/m^3	100

5.4. Application Mode: Diffusion (di2)

Application mode type: Diffusion

Application mode name: di2

5.4.1. Application Mode Properties

Property	**Value**
Default element type	Lagrange - Quadratic
Analysis type	Transient
Frame	Frame (ref)
Weak constraints	Off

5.4.2. Variables

Dependent variables: NH2

Shape functions: shlag(2,'NH2')

Interior boundaries not active

5.4.3. Boundary Settings

Point		1, 3	2
style	mol/m^3	{0,{0,0,0}}	**{0,{0,255,0}}**

5.4.4. Subdomain Settings

Subdomain		1	2
Shape functions (shape)		**shlag(2,'NH2')**	**shlag(2,'NH2')**
Integration order (gporder)		**4**	**4**
Constraint order (cporder)		**2**	**2**
Diffusion coefficient (D)	m^2/s	**DH2**	**DH2poly**
Reaction rate (R)	mol/(m^3·s)	**-(-KH1*NH^2+KH2*NH2)**	0

5.5. Application Mode: Weak Form, Boundary (wb)

Application mode type: Weak Form, Boundary

Application mode name: wb

5.5.1. Application Mode Properties

Property	**Value**
Default element type	Lagrange - Quadratic
Wave extension	Off
Weak constraints	Off
Frame	Frame (ref)

5.5.2. Variables

Dependent variables: Nit, Nit_t

Shape functions: shlag(2,'Nit')

Interior boundaries not active

5.5.3. Boundary Settings

Point	1
Shape functions (shape)	**1**
weak term (weak)	**'Nit_test*Reaction'**
dweak term (dweak)	**'Nit_test*Nit_time'**

6. Solver Settings

Solve using a script: off

Analysis type	Transient
Auto select solver	On
Solver	Time dependent
Solution form	Automatic
Symmetric	Auto
Adaption	Off

6.1. Direct (SPOOLES)

Solver type: Linear system solver

Parameter	**Value**
Pivot threshold	0.1
Preordering algorithm	Minimum degree

6.2. Time Stepping

Parameter	**Value**
Times	0:1e-1:2000
Relative tolerance	0.01
Absolute tolerance	0.0010
Times to store in output	Specified times

Time steps taken by solver	Free
Manual tuning of step size	Off
Initial time step	0.0010
Maximum time step	1.0
Maximum BDF order	5
Singular mass matrix	Maybe
Consistent initialization of DAE systems	Backward Euler
Error estimation strategy	Include algebraic
Allow complex numbers	Off

6.3. Advanced

Parameter	**Value**
Constraint handling method	Elimination
Null-space function	Automatic
Assembly block size	5000
Use Hermitian transpose of constraint matrix and in symmetry detection	Off
Use complex functions with real input	Off
Stop if error due to undefined operation	On
Type of scaling	Automatic
Manual scaling	
Row equilibration	On
Manual control of reassembly	Off
Load constant	On
Constraint constant	On
Mass constant	On

Damping (mass) constant	On
Jacobian constant	On
Constraint Jacobian constant	On

7. Postprocessing

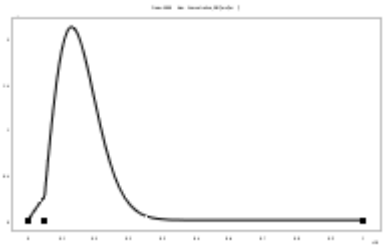

8. Variables

8.1. Boundary

8.1.1. Boundary 1-2

Name	Description	Expression
ndflux_NH_di	Normal diffusive flux, NH	nx_di * dflux_NH_di
ndflux_NH2_di2	Normal diffusive flux, NH2	nx_di2 * dflux_NH2_di2

8.1.2. Boundary 3

Name	Description	Expression
ndflux_NH_di	Normal diffusive flux, NH	
ndflux_NH2_di2	Normal diffusive flux, NH2	nx_di2 * dflux_NH2_di2

8.2. Subdomain

8.2.1. Subdomain 1

Name	Description	Expression
grad_NH_di	Concentration gradient, NH	NHx
dflux_NH_di	Diffusive flux, NH	-D_NH_di * NHx
grad_NH2_di2	Concentration gradient, NH2	NH2x

dflux_NH2_di2	Diffusive flux, NH2	-D_NH2_di2 * NH2x

8.2.2. Subdomain 2

Name	Description	Expression
grad_NH_di	Concentration gradient, NH	
dflux_NH_di	Diffusive flux, NH	
grad_NH2_di2	Concentration gradient, NH2	NH2x
dflux_NH2_di2	Diffusive flux, NH2	-D_NH2_di2 * NH2x

REFERENCES

[1] Robert Doering and Yoshio Nishi "Handbook of Semiconductor Manufacturing Technology" CRC Press 2008

[2] MCGraw-Hill "Semiconductor Manufacturing Handbook" Hwaiyu Geng, 2005.

[3] S.MAY and M.SZE "Fundamentals of Semiconductor Fabrication" John Wiley & Sons, 2003.

[4] H. Nishikawa., "Structures and Properties of Amorphous Silicon — Issues on the Reliability and Novel Applications." from Silicon-Based Materials and Devices: Properties and Devices, Vol. 2. U.S. Naiwa, Academic Press. USA,

[5] W. Goes and T. Grasser, "Charging and Discharging of Oxide Defects in Reliability Issues" IEEE Trans.Dev.Mat.Rel., vol. 8, no. 3, pp. 491–500, 2007.

[6] J.P. Campbell, P.M. Lenahan, C.J. Cochrane, A.T. Krishnan, and S. Kr-ishnan, "Atomic-Scale Defects Involved in the Negative-Bias Temperature Instability," IEEE Trans.Dev.Mat.Rel., vol. 7, no. 4, pp. 540–557,2007

[7] C.H. Helms and E.H. Poindexter, "The Silicon-Silicon-Dioxide System: Its Microstructure and Imperfections," Rep.Prog.Phys., vol. 57, pp. 791–852, 1994

[8] H. Witham and M. Lenahan "The nature of the deep hole trap in mos oxides" IEEE Transactions on Nuclear Science, Vol. NS-34, No. 6, December 1987

[9] J.F. Zhang, C.Z. Zhao, A.H. Chen, G. Groeseneken, and R. De-graeve, "Hole Traps in Silicon Dioxides - Part I: Properties," IEEE Trans.Electr.Dev., vol. 51, no. 8, pp. 1267–1273, 2004.

[10] Jian F. Zhang, Ce Z. Zhao, Ai H. Chen, Guido Groeseneken "Hole-Traps in Silicon Dioxides—Part II: Generation Mechanism" IEEE Trans.Electr.Dev., vol. 51, no. 8, 2004.

[11] D. K. Schroder, "Negative bias temperature instability: What do we understand?" Microelectron. Reliab., vol. 47, no. 6, pp. 841-852, Jun. 2007.

[12] Daniel M. Fleetwood, "Border Traps in MOS Devices", IEEE Transaction on Nuclear Science. vol. 39, no. 2, April 1992

[13] V. Huard, M. Denais, and C. Parthasarathy, “NBTI Degradation: From Physical Mechanisms to Modelling,” Microelectr.Reliab., vol. 46, no. 1,pp. 1–23, 2006.

[14] V. Huard, M. Denais "A thorough investigation of MOSFETs NBTI degradation", Microelectronics Reliability vol. 45,pp. 83–98, 2005

[15] H. Reisinger, O. Blank, W. Heinrigs, A. Mühlhoff, W. Gustin, and C. Schlünder, “Analysis of NBTI degradation- and recovery-behavior based on ultrafast V_T-measurement,” in Proc. IRPS, 2006, pp. 448-453.

[16] M. Ershov, S. Saxena, H. Karbasi, S. Winters, S. Minehane, J. Babcock, R. Lindley, P. Clifton, M. Redford, and A. Shibkov, “Dynamic recovery of negative bias temperature instability in p-type metal-oxide-semiconductor field-effect transistors,” Appl. Phys. Lett., vol. 83, no. 8, pp. 1647-1649, Aug. 2003.

[17] T. Grasser, P.-J, Wagner, Ph. Hehenberger, W. Goes, and B. Kaczer,“A Rigorous Study of Measurement Techniques for Negative Bias Temperature Instability,” IEEE Trans.Dev.Mat.Rel., vol. 8, no. 3, pp.526 – 535, 2008.

[18] GUIDO GROESENEKEN et al, "A reliable approach to charge pumping measurements in MOS transistors", IEEE Transactions on Electron Devices, vol. 1, no. 1, pp.42-53, 1984

[19] J. S. Brugler a’nd P.G:L Jespers, “Charge pumping th MOS devices,” IEEE Trans. Electron Devices, vol. ED-16, p. 297, 1969

[20] G. A. Du, D. S. Ang, Z. Q. Teo, and Y. Z. Hu, “Ultrafast measurement on NBTI,” IEEE Electron Dev. Lett., vol. 30, no. 3, pp. 275-277, Mar. 2009.

[21] Z.Q.Teo, D.S. Ang, and K.S. See "Can the Reaction-Diffusion Model Explain Generation and Recovery of Interface States Contributing to NBTI? ", in IEDM Tech. Dig., pp. 737-740 2009.

[22] Z. Q. Teo, D.S. Ang, and C.M. Ng "Separation of Hole Trapping and Interface-State Generation by Ultrafast Measurement on Dynamic Negative-Bias Temperature Instability ", IEEE Electron Device Letters, vol. 31, no. 7, July 2010.

[23] Z. Q. Teo, D. S. Ang, and C. M. Ng, ““Non-hydrogen-transport” characteristics of dynamic negative-bias temperature instability,” IEEE Electron Dev., Lett., vol. 31, no. 4, pp. 269-271, Apr. 2010.

[24] D. S. Ang, S. Wang, G. A. Du, and Y. Z. Hu, “A consistent deep-level hole trapping model for negative-bias temperature instability,” IEEE Trans. Dev. Mat. Reliab., vol. 8, no. 1, pp. 22-34, Mar. 2008.

[25] J. H. Stathis and S. Zafar, “The negative bias temperature instability in MOS Devices: A review,” Microelectron. Reliab., vol. 46, no. 2–4,pp. 270–286, Feb.–Apr. 2006.

[26] M. A. Alam and S. Mahapatra, “A comprehensive model of PMOS NBTI degradation,” Microelectron. Reliab., vol. 45, no. 1, pp. 71–81, Jan. 2005.

[27] S. Mahapatra, P. B. Kumar, and M. A. Alam, “Investigation and modeling of interface and bulk trap generation during negative bias temperature instability of p-MOSFETs,” IEEE Trans. Electron Devices, vol. 51, no. 9, pp. 1371–1379, Sep. 2004

[28] M. A. Alam, H. Kufluoglu, D. Varghese, and S. Mahapatra, “A comprehensive model for PMOS NBTI degradation: Recent progress,” Micro-electron. Reliab., vol. 47, no. 6, pp. 853–862, Jun. 2007.

[29] S. Mahapatra, P. B. Kumar, T. R. Dalei, D. Saha, and M. A. Alam, “Mechanism of negative bias temperature instability in CMOS devices: Degradation, recovery and impact of nitrogen,” in IEDM Tech. Dig., pp. 105–108, Dec. 2004.

[30] Alvin W. Strong Ernest Y. Wu "Reliability Wearout Mechanisms In Advanced CMOS Technologies", IEEE. A JOHN WILEY & SONS, INC., Publication 2009

[31] S. Rangan, N. Mielke, and E. C. C. Yeh, “Universal recovery behavior of negative bias temperature instability in PMOSFETs,” in IEDM Tech. Dig., pp. 14.3.1–14.3.4, 2003.

[32] V. Huard, F. Monsieur, G. Ribes, and S. Bruyere, “Evidence for hydrogen-related defects during NBTI stress in p-MOSFETs,” in Proc. IRPS, 2003, pp. 178-182.

[33] B. Kaczer, V. Arkhipov, M. Jurczak, and G. Groeseneken, “Negative bias temperature instability (NBTI) in SiO2 and SiON gate dielectrics understood through disorder-controlled kinetics,” Microelectron. Eng., vol. 80, pp. 122-125, 2005

[34] S. Mahapatra, P. B. Kumar, T. R. Dalei, D. Saha, and M. A. Alam, “Mechanism of negative bias temperature instability in CMOS devices: Degradation, recovery and impact of nitrogen,” in IEDM Tech. Dig., pp. 105–108, 2004.

[35] T. Grasser, B. Kaczer, W. Goes, Th. Aichinger, Ph. Hehenberger, and M. Nelhiebel, “A two-stage model for negative bias temperature instability,” in Proc. IRPS, pp. 33-44, 2009.

[36] Patrick M. Lenahan, Jason P. Campbell, Anand T. Krishnan, and Srikanth Krishnan "A Model for NBTI in Nitrided Oxide MOSFETs Which Does Not Involve Hydrogen or Diffusion", IEEE Trans. Electron Devices, vol. 11, no. 2, pp. 219–226, 2011.

[37] D. S. Ang, S. Wang, and C. H. Ling, “Evidence of two distinct degradation mechanisms from temperature dependence of negative bias stressing of the ultra-thin gate P-MOSFET,” IEEE Electron Dev. Lett., vol. 26, no. 12, pp. 906-908, Dec. 2005.

.

[38] D. S. Ang, Z. Q. Teo, J. Ho, and C. M. Ng "Reassessing the Mechanisms of Negative-Bias Temperature Instability by Repetitive Stress/Relaxation Experiments", IEEE Trans. Electron Devices, vol. 11, no. 1, pp. 19–34, 2011.

[39] P.M. Lenahan T. D.Mishima, J. Jumper T. N. Fogarty and R. T. Wilkins "Direct Experimental Evidence for Atomic Scale Structural Changes Involved in the Interface-Trap Transformation Process", IEEE Trans. Nuclear Science, vol. 48, no. 6, pp. 2131–2135, 2001.

[40] A. T. Krishnan, C. Chancelor, S. Chakravarthi, P. E. Nicollian, V. Reddy, and A. Varghese, “Material dependence of hydrogen diffusion: Implica-tion for NBTI degradation,” in IEDM Tech. Dig., pp. 688–691 2005

[41] Haldun Küflüoglu, , and Muhammad Ashraful Alam "A Generalized Reaction–Diffusion Model With Explicit H–H2 Dynamics for Negative-Bias Temperature-Instability (NBTI) Degradation", IEEE Trans. Electron Devices, vol. 54, no. 5, pp. 1101–1107, 2007.

[42] Tibor Grasser and Siegfried Selberherr "Modeling of negative bias temperature instability", Journal of Telecommunications and Information Technology 2007

[43] Sanjay V. Kumar, Chris H. Kim, and Sachin S. Sapatnekar "A Finite-Oxide Thickness-Based Analytical Model for Negative Bias Temperature Instability," IEEE Trans. Electron Devices, vol. 9, no. 4, pp. 537–556, 2009.